Geophys. J. Int. (2007) **170,** 823–838 doi: 10.1111/j.1365-246X.2007.03462.x

Second order homogenization of the elastic wave equation for non-periodic layered media

Y. Capdeville[1] and J.-J. Marigo[2]

[1] *Équipe de sismologie, Institut de Physique du Globe de Paris, CNRS Paris, France. E-mail: capdevil@ipgp.jussieu.fr*
[2] *Laboratoire de Modélisation en Mécanique (UMR* 7607*), Université Paris VI, Paris, France*

Accepted 2007 March 30. Received 2007 March 29; in original form 2006 Nonember 13

SUMMARY

In many cases, in the seismic wave propagation modelling context, scales much smaller than the minimum wavelength are present in the earth model in which we wish to compute seismograms. For many numerical methods these small scales are a challenge leading to high numerical cost. The purpose of this paper is to understand and to build the effective medium and equations allowing to average the small scales of the original medium without losing the accuracy of the wavefield computation. In this paper, only the simple layered medium case is studied, leaving the general 3-D medium case for future work. To obtain such an effective medium and equations, we use high order two scale homogenization applied to the wave equation for layered media with rapid variation of elastic properties and density compared to the smallest wavelength of the wavefield. We show that the order 0 homogenization gives the result that was obtained by Backus in 1962. Order 0 homogenized models are transversely isotropic even though the original model is isotropic. It appears that order 0 is not enough to obtain surface waves with correct group and phase velocities and higher order homogenization terms up to two are often required. In many cases, the order one and two simply require to correct the boundary conditions of the wave equation to obtain an accurate solution, even for surface waves. We show how to extend the theory from the periodic case to the non-periodic case. Examples in periodic and non-periodic media are shown. The accuracy of the results obtained by homogenization is checked against the normal mode solution computed in the original medium and shows good agreement.

Key words: homogenization, global seismology, normal modes, numerical modeling, surface waves.

1 INTRODUCTION AND MOTIVATIONS

One important problem in seismology is to compute the response of the Earth recorded anywhere on the Earth for a given earth model and some earthquake parameters. This is the forward problem. Another important problem is, knowing the forward problem, being able to find models that explain the data. This is the inverse problem. For both problems, being able to model the wavefield is required. The numerical cost of most modelling techniques is directly related to the maximum frequency of the wavefield and to the smallest details of the elastic model. Therefore, the modelling is possible because it is assumed that very small scales have no effect, or a minor one, on long periods of seismograms. For example, if a millimetre scale heterogeneity had a dramatic influence on a 100 s period and longer seismogram, there would be no hope for seismology because the computational cost would be out of reach. In other words, one of the basic assumptions in seismology is that scales can be separated. Nevertheless, even if this assumption of scale separation is widely used, the upscaling rules allowing us to go from small scales to effective large scales have been little studied for the wave equations in the seismological community. Effects of randomly distributed scatterers have been widely studied (e.g. Aki & Richards 1980), but does not provide upscaling rules or effective media and equations in the case of deterministic rapidly varying structure with elastic property contrasts of arbitrary amplitude.

Before going further, let us give two typical examples for which upscaling rules are implicitly used. In the tomography seismic imaging field, different research groups obtain different seismic velocity models of the same region (e.g. the Earth) at different resolution lengths. In order to compare these different models, only the common longest scales of different models are used. To remove the smaller scales of some of the models, an averaging with the appropriate spacial filter is performed. In this case, the upscaling rule used to find the effective model is just the average of velocities. An other example for which the scale separation is implicitly used can be found in the forward modelling numerical simulations. Thanks to the recent advance in this domain with numerical methods like the Spectral Element Method (SEM; see e.g. Komatitsch & Vilotte 1998, for one of the first applications of the SEM to seismology), it is now possible to accurately model waveforms in complex 3-D

media. The numerical cost of such method is controlled by the size of the mesh and the time step of time marching scheme. For the usual explicit time marching scheme, the time step is also controlled by the mesh (the time step is proportional to the smallest element size). In homogeneous media, the element size is controlled by the smallest wavelength of the wavefield, and finally the total numerical cost scales as the corner frequency of the source to the power four. If one is only interested in the long- period signal, it is therefore possible to perform relatively inexpensive numerical simulations. If the elastic model is heterogeneous, the minimum wavelength is not the only parameter which controls the element size. Indeed, in order to be accurate, all physical discontinuities of the model have to be matched by mesh element boundaries. Such a mesh can be very difficult to design and the numerical cost can be considerably higher than in the homogeneous case due to the very small elements resulting form the meshing of the interfaces. When the distance between interfaces or any heterogeneities is much smaller that the smallest wavelength, leading to unacceptable numerical cost, classical solutions are either to ignore the interfaces or to average the elastic properties across the interfaces. For the first solution, the upscaling rules is unknown and for the second, the upscaling rules is an average of the elastic properties. Following these examples, a natural question is, what are the upscaling rules or effective media and equations consistent with the wave equation?

An early work on effective media, or upscaling rules, for the wave equation has shown that, in the layered model case, averaging velocities is not consistent with the wave equation and that averaging must be done on non-linear functions of the elastic parameters (Backus 1962). This study shows that the upscaling rules are not trivial. Backus (1962)'s results are nevertheless not sufficient to obtain effective media which provides accurate results, especially for surface waves. While this multiscale problem has not been extensively studied in seismology, it has been widely studied in material mechanics for the static case. Bounds of effective elastic properties for composite elastic materials were derived in the 1960s (Hashin & Shtrikman 1963; Hill 1965). But it is in the periodic case that a large number of results were obtained with the homogenization theory: from the pioneering work of Auriault & Sanchez-Palencia (1977), a large number of studies have been devoted either to the mathematical foundations of the homogenization theory in the static context (e.g. Bensoussan *et al.* 1978; Murat & Tartar 1985; Allaire 1992), or to applications of the effective static behaviour of composite materials (see e.g. Dumontet (1986); Francfort & Murat 1986; Abdelmoula & Marigo 2000; Haboussi, Dumontet & Billoët 2001a,b). In contrast, only a few studies have been devoted to the theory and its applications in the general dynamical context or to the non-periodic cases. However, one can refer to Sanchez-Palencia (1980), Auriault & Bonnet (1985), Moskow & Vogelius (1997) or Allaire & Conca (1998) for the dynamical context or to Briane (1994) for the non-periodic case. Here, we apply these homogenization techniques to extend Backus's (1962) results.

For wave propagation problems, high-order homogenization has been used with success for small-scale period media (e.g. Fish & Chen 2004). It has been shown that effects like dispersion and apparent attenuation effects due to small-scale heterogeneities can be recovered by high-order homogenization. Nevertheless, these studies do not consider on non-periodic media and on surface waves for which the boundary conditions must be studied with care.

The purpose of this paper is to study the upscaling problem in details for the layered medium in a first step, leaving the general 3-D case for future work. Because our main domain of application is the global earth, we work with spherically symmetric models. Nevertheless, all the results presented here can be applied with no modification to the axisymmetric or Cartesian cases. For spherically symmetric models, the normal mode methods classically used in seismology are very efficient and can handle with no difficulty rapidly varying media. Therefore, this work will not be directly of interest to improve such methods. Such a context nevertheless allows to test the accuracy of the effective media and effective equations obtained here by comparing the results obtained by homogenization with results obtained with the normal modes in the original model. The results obtained here will be interesting, however, for inverse problems and for forward modelling problems in model which are varying rapidly in only one direction (such as actual global scale crustal models) and for numerical methods like SEM.

We will first develop the theory assuming a periodic layered medium, which is the classical domain of validity of 'two-scale homogenization' asymptotic theory. To solve our two-scale problem in a 1-D medium we rewrite the wave equations as a first-order system of equations similarly to the classical approach used for normal mode methods in such media. Doing so, on one hand, considerably simplifies the two-scale homogenization calculation but, on the other hand, makes the results more difficult to interpret for readers not familiar with normal mode techniques. Moreover, results are obtained here in the spectral domain and, in order to be applied to other numerical techniques, such as SEM, they need to be converted first to the physical domain which is not straightforward. This will be the purpose of future works. The accuracy of the results is tested against the normal mode solution in the original model as the reference solution. The results obtained in the periodic case are then extended to the non-periodic case and again tested against the normal mode solution in the original model.

2 PRELIMINARY: SOLVING THE WAVE EQUATION IN 1-D MEDIA

We consider a finite domain $\mathbf{\Omega}$ of boundary $\partial\mathbf{\Omega}$. When gravity and anelasticity are not taken into account, the wave equation can be written

$$\rho\ddot{\mathbf{u}} - \boldsymbol{\nabla}\cdot\boldsymbol{\sigma} = \mathbf{f} \tag{1}$$

$$\boldsymbol{\sigma} = \mathbf{c} : \boldsymbol{\epsilon}(\mathbf{u}), \tag{2}$$

where ρ is the density, $\mathbf{u}$ the displacement field, $\ddot{\mathbf{u}}$ the acceleration field, $\boldsymbol{\sigma}$ the stress tensor, $\mathbf{f}$ the source force, $\mathbf{c}$ the fourth order elastic tensor, : the double indices contraction and $\boldsymbol{\epsilon}(\mathbf{u}) = \frac{1}{2}(\boldsymbol{\nabla}\mathbf{u} + {}^T\boldsymbol{\nabla}\mathbf{u})$ the strain tensor with T the transpose operator. We impose a free surface boundary condition on $\partial\mathbf{\Omega}$, $\boldsymbol{\sigma}\cdot\mathbf{n} = 0$, where $\mathbf{n}$ is the normal vector to $\partial\mathbf{\Omega}$. We assume that $\mathbf{f}$ both depends upon time and space, but we assume that the density and elastic properties are not time dependent.

In this paper, we limit our work to layered media, in other words to 1-D media. All the examples and validation tests presented in this paper are performed in spherically symmetric global earth models of radius r_Ω. We therefore use a spherical coordinates system $\mathbf{r} = (r, \theta, \phi)$ where r is the radius, θ the co-latitude and ϕ the longitude. This is absolutely not a limitation and all results presented here can be applied without modification to Cartesian or cylindrical coordinate systems for other types of layered models. For spherically symmetric layered media, we have $\mathbf{c}(\mathbf{r}) = \mathbf{c}(r)$ and $\rho(\mathbf{r}) = \rho(r)$.

For such 1-D models, the normal mode method is a classical and efficient way to solve the wave equations. It is performed in two steps: first, a basis of eigenfrequencies ω_k and eigenfunctions $\mathbf{u}_k$ of

the solution space is found by solving the wave eqs. (1) and (2) in the frequency domain with $\mathbf{f} = 0$:

$$\boldsymbol{\nabla} \cdot \boldsymbol{\sigma}_k = -\omega_k^2 \rho \mathbf{u}_k \tag{3}$$

$$\boldsymbol{\sigma}_k = \mathbf{c} : \boldsymbol{\epsilon}(\mathbf{u}_k). \tag{4}$$

Second, once the eigenfunctions $\{\mathbf{u}_k, k \in \mathbb{N}\}$ basis is found, the solution for a given source $\mathbf{f}$ can easily be computed using an expansion on this basis.

Assuming a 1-D model with a vertical symmetry axis, the solution to (3) and (4) with free surface conditions is often sought in the spectral domain for the horizontal directions. (e.g. Takeuchi & Saito 1972). For spherically symmetric models, we use

$$\begin{aligned}\mathbf{u}(\mathbf{r}, \omega) = \big[& U_l^m(r, \omega)\mathbf{e}_r + V_l^m(r, \omega)\boldsymbol{\nabla}_1 \\ & - W_l^m(r, \omega)(\mathbf{e}_r \times \boldsymbol{\nabla}_1)\big] Y_l^m(\theta, \phi),\end{aligned} \tag{5}$$

where $(\mathbf{e}_r, \mathbf{e}_\theta, \mathbf{e}_\phi)$ is the spherical coordinate unit vector set, $\boldsymbol{\nabla}_1$ is the gradient operator on the unit sphere, Y_l^m the spherical harmonic of angular order l and azimuthal order m (e.g. Dahlen & Tromp 1998). $\frac{\sqrt{l(l+1)}}{r}$ can be seen as the horizontal wave number. The radial traction $\mathbf{T} = \boldsymbol{\sigma} \,.\, \mathbf{e}_r$ can also be written under the form

$$\begin{aligned}\mathbf{T}(\mathbf{r}, \omega) = \big[& T_{U_l}^m(r, \omega)\mathbf{e}_r + T_{V_l}^m(r, \omega)\boldsymbol{\nabla}_1 \\ & - T_{W_l}^m(r, \omega)(\mathbf{e}_r \times \boldsymbol{\nabla}_1)\big] Y_l^m(\theta, \phi).\end{aligned} \tag{6}$$

Using (5) and (6) into (3) and (4), we obtain for each l, two independent systems of equations, one for $(U_l, T_{U_l}, V_l, T_{V_l})$ (spheroidal case) and one for (W_l, T_{W_l}) (toroidal case), independent of m, that can be rewritten as a first-order system of equations:

$$\frac{\partial_q \boldsymbol{\mathcal{Y}}_l}{\partial r}(r, \omega) = {}_q\mathbf{A}_l(r, \omega)\, {}_q\boldsymbol{\mathcal{Y}}_l(r, \omega), \tag{7}$$

where q can take two values, s for the spheroidal problem, t for the toroidal problem,

$${}_s\boldsymbol{\mathcal{Y}}_l = {}^T(r U_l, r T_{U_l}, r\gamma_l V_l, r\gamma_l T_{V_l}), \tag{8}$$

for the spheroidal case and

$${}_t\boldsymbol{\mathcal{Y}}_l = {}^T(r W_l, r T_{W_l}), \tag{9}$$

for the toroidal case, with $\gamma_l = \sqrt{l(l+1)}$. Expressions for ${}_q\,\mathbf{A}_l$ matrices can be found in Takeuchi & Saito (1972), Aki & Richards (1980) or in Appendix A. Solutions must be regular at $r = 0$ and the free surface boundary conditions impose that radial traction components of ${}_s\boldsymbol{\mathcal{Y}}_l$ and ${}_t\boldsymbol{\mathcal{Y}}_l$ must vanish for $r = r_\Omega$:

$$[{}_s\boldsymbol{\mathcal{Y}}_l(r_\Omega, \omega)]_2 = [{}_s\boldsymbol{\mathcal{Y}}_l(r_\Omega, \omega)]_4 = [{}_t\boldsymbol{\mathcal{Y}}_l(r_\Omega, \omega)]_2 = 0, \tag{10}$$

where $[.]_i$ is the i^{th} component of a vector. In the following, we forget indices ${}_t$ and ${}_s$ if expressions are the same for spheroidal and toroidal problems. The l index is also omitted in most of the expressions. Before applying boundary conditions, (7) has four independent solutions for the spheroidal case and two for the toroidal case. Only two solutions are regular at the centre of the Earth for the spheroidal case and one for the toroidal case. The free surface boundary condition can only be met for a discrete set of eigenfrequencies. For the toroidal case, an eigenfrequency is found when the traction at the surface vanishes and, for the spheroidal case, when the determinant of the traction component of the two remaining solutions at the surface,

$$m_5 = r^2\gamma_l \left(T_U^{(1)} T_V^{(2)} - T_V^{(1)} T_U^{(2)} \right), \tag{11}$$

vanishes. A classical procedure to solve (7) with the boundary conditions (10) is, for a fixed frequency and a given l, to start from an analytical solution close to the Earth's centre, then to integrate (7) with a Runge–Kutta scheme up to the surface. The next step is to find eigenfrequencies for which the traction vanishes at the free surface with a shooting method. For the spheroidal case, the procedure can be complicated by numerical instabilities. A solution to this problem is to solve equations for the minors of the two solutions regular at $r = 0$ (see Woodhouse 1988) instead of the original system. In that case, the equations can still be written under the form (7), but the system is stable. One especially important minor is (11) because it vanishes for $r = r_\Omega$ when an eigenfrequency is found. For each problem q and each angular degree l and in a finite frequency band, a finite number of eigenfrequencies are found noted by an index n. The index k of the eigenfrequency ω_k represents (q, n, l). Once an ω_k is found, the corresponding eigenfunction $\mathbf{u}_k$ can be computed. Actually, for each eigenfrequency there are $2l + 1$ eigenfunctions because they also depend on the azimuthal order m. In the following, we forget this complication and note ω_k and $\mathbf{u}_k$ with the same index.

Once the eigenfunction basis is known, expanding the solution for a given source and computing it back in the time domain is straightforward. For example, if $\mathbf{f}(\mathbf{r}, t)$ can be written as $\mathbf{f}(r)H(t)$, where H is the Heaviside function, we have

$$\mathbf{u}(\mathbf{r}, t) = \sum_k \mathbf{u}_k \left(\int_\Omega \mathbf{u}_k^\star . \mathbf{f}\, d\Omega \right) \frac{1 - \cos(\omega_k t)}{\omega_k^2} H(t), \tag{12}$$

where* is the complex conjugate. Moreover, if $\mathbf{f}$ is a double couple point source located in $\mathbf{r}_s$,

$$\int_\Omega \mathbf{u}_k^\star . \mathbf{f}\, d\Omega = \boldsymbol{\epsilon}_k^\star(\mathbf{r}_s) : \mathbf{M}, \tag{13}$$

where $\mathbf{M}$ is the earthquake moment tensor, $\boldsymbol{\epsilon}_k = \boldsymbol{\epsilon}(\mathbf{u}_k)$.

This normal mode approach of the wave equations is widely used in the seismological community, thanks to its efficiency and accuracy. Because of this efficiency, normal mode methods can handle models with very fast radial variations of the elastic properties compared to the wavelength. Therefore, for layered media, even with fast variations, homogenization is not required to solve the wave equation. Nevertheless, homogenization will be very important for other methods like SEM and for inverse problems. Working with the normal mode technique allows us to perform quickly some experiments to test the validity of homogenization.

3 TWO-SCALE HOMOGENIZATION IN LAYERED PERIODIC MEDIA

3.1 Theoretical development

We assume in this section that the variation of the elastic and density properties along the r axis are λ_m-periodic, that is $\mathbf{c}(r + \lambda_m) = \mathbf{c}(r)$ and $\rho(r + \lambda_m) = \rho(r)$ for all r. We also assume that there exists a smallest wavelength λ_c for the wavefield $\mathbf{u}$. This is a reasonable assumption away from the near field and for a typical source term $\mathbf{f}(\mathbf{r}, \omega)$ with a limited frequency band with a corner frequency ω_c. We finally assume that the periodicity of the oscillations of the model is much smaller than the wavelength of the wavefield: $\varepsilon = \frac{\lambda_m}{\lambda_c} \ll 1$. With this last assumption, the wavefield is sensitive to the fast oscillations of the model only in an effective way. The aim of this paper is to define the effective medium and equations and to explore its potential accuracy, with a special focus on surface waves. The operator $\mathbf{A}$ depends on ε since it depends on λ_m. We note this dependence with an upper script: $\mathbf{A}^\varepsilon$ as well as $\boldsymbol{\mathcal{Y}}^\varepsilon$ solution of:

$$\frac{\partial \boldsymbol{\mathcal{Y}}^\varepsilon}{\partial r}(r, \omega) = \mathbf{A}^\varepsilon(r, \omega)\boldsymbol{\mathcal{Y}}^\varepsilon(r, \omega). \tag{14}$$

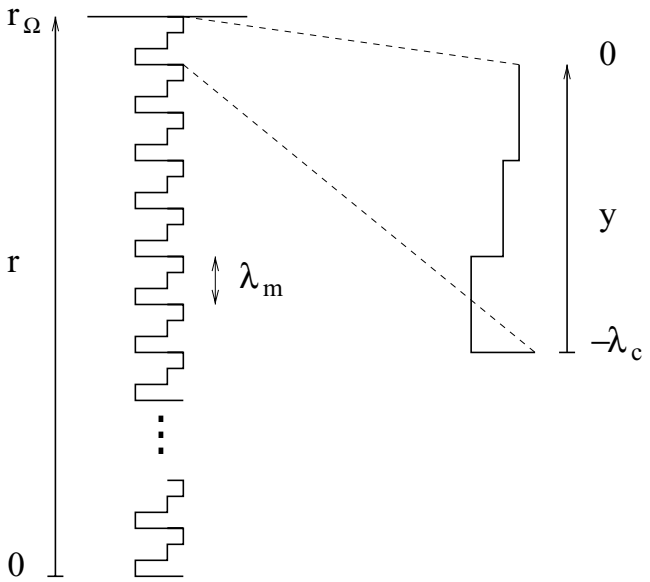

Figure 1. Sketch showing on the left the rapid periodic variation with depth of an elastic parameter or the density of the model and on the right, a zoom on one periodic cell.

In what follows, we postpone the discussion on the frequency and the eigenfrequencies search to the end of this section. Assuming a fixed frequency, the dependence of operators and vectors on ω is omitted. To avoid difficulties with the free surface boundary condition which may be not compatible with this fixed frequency, we leave open the centre of the Earth boundary condition (regularity) until the end of the section. Doing so, all frequencies are solutions.

In the classical two-scale homogenization (e.g. Bensoussan *et al.* 1978; Allaire 1992), two space variables are used:

(i) the macroscopic variable which is the original space variable and here is r;

(ii) the microscopic variable, $y = \frac{r - r_\Omega}{\varepsilon}$ (see Fig. 1. Because $\varepsilon \ll 1$, y is a kind of zoom to the fine scales. The goal of the $-r_\Omega$ in the y definition is to have $y = 0$ on the Earth free surface.

We define:

$$\mathbf{S}\left(r, \frac{r - r_\Omega}{\varepsilon}\right) = \mathbf{S}(r, y) = \mathbf{A}^\varepsilon(r). \tag{15}$$

In spherical coordinates, $\mathbf{A}^\varepsilon$ is not exactly λ_m-periodic because of coefficients of the form r^{-n} (see Appendix A). Nevertheless, when ε is small and we are far away enough from the Earth's centre, $\mathbf{A}^\varepsilon(r)$ is quasi periodic. In the following, the r dependency in $\mathbf{S}$ is omitted.

We assume that $\boldsymbol{\mathcal{Y}}^\varepsilon$ for a given value of ε and a given ω depends on both the macroscopic scale and microscopic scale and that it can be expanded in the form:

$$\boldsymbol{\mathcal{Y}}^\varepsilon(r) = \sum_{i=-1}^{+\infty} \varepsilon^i \boldsymbol{\mathcal{Y}}^i\left(r, \frac{r - r_\Omega}{\varepsilon}\right). \tag{16}$$

(We shall see later why the sum starts at $i = -1$). In the limit $\varepsilon \rightharpoonup 0$, one can think about r as a constant parameter with respect to y: in that limit, we assume the scales can be separated and we now treat r and y as independent variables. With this assumption, derivatives with respect to r become:

$$\frac{\partial}{\partial r} \to \frac{\partial}{\partial r} + \frac{1}{\varepsilon}\frac{\partial}{\partial y}. \tag{17}$$

Because there is a radial derivative in the relation between stress and displacement, if the power expansion in ε of the displacement starts at 0, it makes sense to start the power expansion for the stress at -1. Because the vector $\boldsymbol{\mathcal{Y}}$ contains both displacement and traction components, its power expansion (16) starts at -1. If we explicit this expansion in the toroidal case, we have

$${}_t\boldsymbol{\mathcal{Y}}^\varepsilon = r\begin{pmatrix} W^\varepsilon \\ T_W^\varepsilon \end{pmatrix} = \frac{r}{\varepsilon}\begin{pmatrix} 0 \\ T_W^{-1} \end{pmatrix} + r\begin{pmatrix} W^0 \\ T_W^0 \end{pmatrix} + \varepsilon r\begin{pmatrix} W^1 \\ T_W^1 \end{pmatrix} + \dots \tag{18}$$

with similar expressions in the spheroidal case.

Introducing (17) and (16) in (14) and identifying each coefficient of the power expansion in ε to zero, we obtain the following sequence of equations:

$$\frac{\partial \boldsymbol{\mathcal{Y}}^i}{\partial r} + \frac{\partial \boldsymbol{\mathcal{Y}}^{i+1}}{\partial y} = \mathbf{S}\boldsymbol{\mathcal{Y}}^i, \tag{19}$$

with the boundary conditions

$$\left[{}_s\boldsymbol{\mathcal{Y}}^i(r_\Omega, 0)\right]_2 = \left[{}_s\boldsymbol{\mathcal{Y}}^i(r_\Omega, 0)\right]_4 = \left[{}_t\boldsymbol{\mathcal{Y}}^i(r_\Omega, 0)\right]_2 = 0. \tag{20}$$

We now need to solve this sequence of equations starting at $i = -2$. For that purpose, we first introduce the *cell* average $\langle g\rangle$ for any function $g(r, y)$:

$$\langle g\rangle(r) = \frac{1}{\lambda_c}\int_0^{\lambda_c} g(r, y)\, dy, \tag{21}$$

with $\lambda_c = \frac{\lambda_m}{\varepsilon}$. We define the variation $\bar{g}$ of any function g with respect to its average, $\bar{g}(r, y) = g(r, y) - \langle g\rangle(r)$. In the rest of the paper, we name $\bar{g}$ the correction to the average $\langle g\rangle$ of the function g. We will need the two following properties for any function $g(r, y)$, λ_c-periodic in y:

$$\left\langle \frac{\partial g}{\partial y} \right\rangle = 0, \text{ and} \tag{22}$$

$$\frac{\partial g}{\partial y} = 0 \Leftrightarrow g(r, y) = g(r) = \langle g\rangle. \tag{23}$$

The first one can easily be demonstrated using the Green formula and the periodicity over y and the second is straightforward.

3.1.1 Order ε^{-2}

For $i = -2$, (19) gives $\partial\boldsymbol{\mathcal{Y}}^{-1}/\partial y = 0$. Using (23), we therefore have $\boldsymbol{\mathcal{Y}}^{-1} = \langle\boldsymbol{\mathcal{Y}}^{-1}\rangle$.

3.1.2 Order ε^{-1}

For $i = -1$(19), gives:

$$\frac{\partial \boldsymbol{\mathcal{Y}}^{-1}}{\partial r} + \frac{\partial \boldsymbol{\mathcal{Y}}^{0}}{\partial y} = \mathbf{S}\boldsymbol{\mathcal{Y}}^{-1}. \tag{24}$$

Taking the cell average of the last equation, using $\boldsymbol{\mathcal{Y}}^{-1} = \langle\boldsymbol{\mathcal{Y}}^{-1}\rangle$ and (22), we have

$$\frac{\partial \boldsymbol{\mathcal{Y}}^{-1}}{\partial r} = \langle\mathbf{S}\rangle\boldsymbol{\mathcal{Y}}^{-1}. \tag{25}$$

Knowing the particular form of $\boldsymbol{\mathcal{Y}}^{-1}$(displacement components are 0), using the $\mathbf{S}$ expressions and the boundary conditions, one can check that the only solution to (25) is $\boldsymbol{\mathcal{Y}}^{-1} = 0$. Therefore, (24) also gives

$$\frac{\partial \boldsymbol{\mathcal{Y}}^{0}}{\partial y} = 0, \tag{26}$$

which, using (23) gives $\mathcal{Y}^0 = \langle \mathcal{Y}^0 \rangle$. This an important result: in the layered case, the displacement and the radial traction at order 0 do not depend on the microscopic variable y.

3.1.3 Order ε^0

For $i = 0$(19), gives

$$\frac{\partial \mathcal{Y}^0}{\partial r} + \frac{\partial \mathcal{Y}^1}{\partial y} = \mathbf{S}\mathcal{Y}^0. \tag{27}$$

Taking the cell average of the last equation, using $\mathcal{Y}^0 = \langle \mathcal{Y}^0 \rangle$ and (22), we obtain the order 0 homogenized equation:

$$\frac{\partial \mathcal{Y}^0}{\partial r} = \langle \mathbf{S} \rangle \mathcal{Y}^0, \tag{28}$$

with the boundary conditions $[{}_s\mathcal{Y}^0(r_{\mathbf{\Omega}})]_2 = [{}_s\mathcal{Y}^0(r_{\mathbf{\Omega}})]_4 = [{}_t\mathcal{Y}^0(r_{\mathbf{\Omega}})]_2 = 0$. The order 0 homogenized eq. (28) has the same form as the original eq. (14) but for different elastic coefficients. As shown in appendix A, $\langle \mathbf{S} \rangle$reproduces the result obtained by Backus (1962). An interesting and well-known result is that the order 0 homogenized model is transversely isotropic (with a vertical symmetry axis) even though the original model is isotropic. From (27) and (28), we also obtain the following equation:

$$\frac{\partial \mathcal{Y}^1}{\partial y} = (\mathbf{S} - \langle \mathbf{S} \rangle)\mathcal{Y}^0. \tag{29}$$

At this stage, we can introduce the first-order periodic corrector matrix $\mathbf{X}^1(y)$, solution of

$$\frac{\partial \mathbf{X}^1}{\partial y}(y) = \mathbf{S}(y) - \langle \mathbf{S} \rangle. \tag{30}$$

$\mathbf{X}^1$ is periodic by construction and, to obtain a unique solution, we impose $\langle \mathbf{X}^1 \rangle = 0$. The dependecy of $\mathbf{X}$ over l and ω is the same as $\mathbf{S}$ (see Appendix A). Thanks to this corrector, once the order 0 solution is found, we can compute the first-order periodic corrections with

$$\tilde{\mathcal{Y}}^1(r, y) = \mathbf{X}^1(y)\mathcal{Y}^0(r). \tag{31}$$

To obtain the solution at the order 1, $\langle \mathcal{Y}^1 \rangle$remains to be found.

3.1.4 Order ε

Taking the cell average (19) for $i = 1$gives

$$\frac{\partial \langle \mathcal{Y}^1 \rangle}{\partial r} = \langle \mathbf{S}\mathcal{Y}^1 \rangle, \tag{32}$$

which, using $\mathcal{Y}^1 = \tilde{\mathcal{Y}}^1 + \langle \mathcal{Y}^1 \rangle$ and (31), can be rewritten:

$$\frac{\partial \langle \mathcal{Y}^1 \rangle}{\partial r} = \langle \mathbf{S} \rangle \langle \mathcal{Y}^1 \rangle + \langle \mathbf{S}\mathbf{X}^1 \rangle \mathcal{Y}^0. \tag{33}$$

This is the first-order homogenized equation. It has the same form as the order 0 (28) with an extra body force term $\langle \mathbf{S}\mathbf{X}^1 \rangle \mathcal{Y}^0$that can be determined with the solution at the order 0. Because $\tilde{\mathcal{Y}}^1$can be different from 0 at the surface, in order to satisfy the correct boundary conditions for $\mathcal{Y}^1 = \langle \mathcal{Y}^1 \rangle + \tilde{\mathcal{Y}}^1$, eq. (33) for $\langle \mathcal{Y}^1 \rangle$must satisfy the following boundary conditions:

$$\left[\langle {}_s\mathcal{Y}^1 \rangle (r_{\mathbf{\Omega}})\right]_2 = -\left[{}_s\mathbf{X}^1(0)\,{}_s\mathcal{Y}^0(r_{\mathbf{\Omega}})\right]_2, \tag{34}$$

$$\left[\langle {}_s\mathcal{Y}^1 \rangle (r_{\mathbf{\Omega}})\right]_4 = -\left[{}_s\mathbf{X}^1(0)\,{}_s\mathcal{Y}^0(r_{\mathbf{\Omega}})\right]_4, \tag{35}$$

$$\left[\langle {}_t\mathcal{Y}^1 \rangle (r_{\mathbf{\Omega}})\right]_2 = -\left[{}_t\mathbf{X}^1(0)\,{}_t\mathcal{Y}^0(r_{\mathbf{\Omega}})\right]_2. \tag{36}$$

After some manipulations, we also get

$$\frac{\partial \mathcal{Y}^2}{\partial y} = \frac{\partial \mathbf{X}^1}{\partial y}\langle \mathcal{Y}^1 \rangle + \frac{\partial \mathbf{X}^2}{\partial y}\mathcal{Y}^0 \tag{37}$$

where $\mathbf{X}^2$ is the second-order periodic corrector matrix, solutions of

$$\frac{\partial \mathbf{X}^2}{\partial y}(y) = \mathbf{S}\mathbf{X}^1 - \mathbf{X}^1\mathbf{S} - \langle \mathbf{S}\mathbf{X}^1 \rangle. \tag{38}$$

$\mathbf{X}^2$ is periodic by construction and is uniquely defined by setting $\langle \mathbf{X}^2 \rangle = 0$. Knowing $\mathcal{Y}^0$ and $\langle \mathcal{Y}^1 \rangle$, we can compute the second-order periodic correction:

$$\tilde{\mathcal{Y}}^2 = \mathbf{X}^1\langle \mathcal{Y}^1 \rangle + \mathbf{X}^2\mathcal{Y}^0. \tag{39}$$

3.1.5 Order ε^2

(19) for $i = 2$, taking the average gives and after some manipulations gives

$$\frac{\partial \langle \mathcal{Y}^2 \rangle}{\partial r} = \langle \mathbf{S} \rangle \langle \mathcal{Y}^2 \rangle + \langle \mathbf{S}\mathbf{X}^1 \rangle \langle \mathcal{Y}^1 \rangle + \langle \mathbf{S}\mathbf{X}^2 \rangle \langle \mathcal{Y}^0 \rangle, \tag{40}$$

with boundary conditions similar to (34–36). We could continue up to any arbitrary large i, but we stop at $i = 2$.

It can be shown that, if $\mathcal{Y}^\varepsilon$ is solution of (14) and $\mathcal{Y}^0$ is solution of (28), then we have $\mathcal{Y}^\varepsilon \rightharpoonup \mathcal{Y}^0$ as $\varepsilon \rightharpoonup 0$ in the weak sense and in the appropriate space (e.g. Murat & Tartar 1985; Allaire 1992). The proof of the convergence of the higher order terms is much more difficult (see however Dumontet (1986) where a convergence result is obtained for the expansion including the boundary layer term).

3.1.6 Combining all orders

We need to solve (28), (33) and (40) with their boundary conditions successively. Because we have an eigenvalue problem when the Earth centre boundary condition (regularity) is taken into account with the free surface boundary condition, the fixed frequency ω assumed at the beginning of this section cannot hold. A solution to solve the problem is to introduce a power expansion in ε of the eigenfrequencies: $\omega_k^\varepsilon = \sum_{i=0}^{i=+\infty} \varepsilon^i \omega_k^i$. Introducing this expansion in the equations (28), (33) and (40) leads to a set of problems allowing to find successively $(\omega_k^0, \mathcal{Y}_k^0)$, then $(\omega_k^1, \mathcal{Y}_k^1)$, *etc*. This approach has been used, for example, in optics (Golowich & Weinstein 2003). Because the next stage of this work is to apply the homogenization technique to classical time space numerical methods, we do not follow this solution here and instead we choose to solve for $\langle \hat{\mathcal{Y}}^2 \rangle$, solution of

$$\frac{\partial \langle \hat{\mathcal{Y}}^2 \rangle}{\partial r} = \left(\langle \mathbf{S} \rangle + \varepsilon \langle \mathbf{S}\mathbf{X}^1 \rangle + \varepsilon^2 \langle \mathbf{S}\mathbf{X}^2 \rangle\right) \langle \hat{\mathcal{Y}}^2 \rangle, \tag{41}$$

with the following boundary conditions

$$\left[\langle {}_s\hat{\mathcal{Y}}^2 \rangle (r_{\mathbf{\Omega}})\right]_2 = -\left[{}_s\hat{\mathbf{X}}^2(0) \langle {}_s\hat{\mathcal{Y}}^2 \rangle (r_{\mathbf{\Omega}})\right]_2, \tag{42}$$

$$\left[\langle {}_s\hat{\mathcal{Y}}^2 \rangle (r_{\mathbf{\Omega}})\right]_4 = -\left[{}_s\hat{\mathbf{X}}^2(0) \langle {}_s\hat{\mathcal{Y}}^2 \rangle (r_{\mathbf{\Omega}})\right]_4, \tag{43}$$

$$\left[\langle {}_t\hat{\mathcal{Y}}^2 \rangle (r_{\mathbf{\Omega}})\right]_2 = -\left[{}_t\hat{\mathbf{X}}^2(0) \langle {}_t\hat{\mathcal{Y}}^2 \rangle (r_{\mathbf{\Omega}})\right]_2, \tag{44}$$

where $\hat{\mathbf{X}}^2 = \varepsilon\mathbf{X}^1 + \varepsilon^2\mathbf{X}^2$. One can check summing (28), (33) and (40) and their corresponding boundary conditions that, up to the second order in ε,

$$\langle \hat{\mathcal{Y}}^2 \rangle = \mathcal{Y}^0 + \varepsilon \langle \mathcal{Y}^1 \rangle + \varepsilon^2 \langle \mathcal{Y}^2 \rangle + O(\varepsilon^3). \tag{45}$$

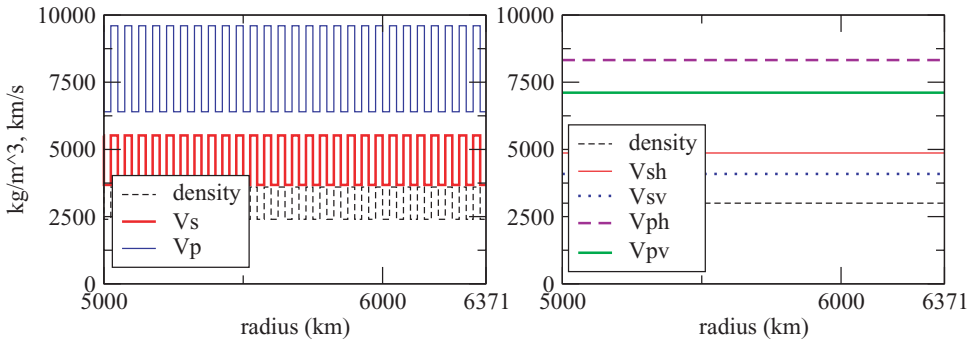

Figure 2. Original onion 1 model. On the left is shown the density, *P*- and *S*-waves velocities as a function of the radius and for the last 1371 km only. The values are constant in each layer and the periodicity is of 50 km. On the right is shown the corresponding order 0 homogenized model.

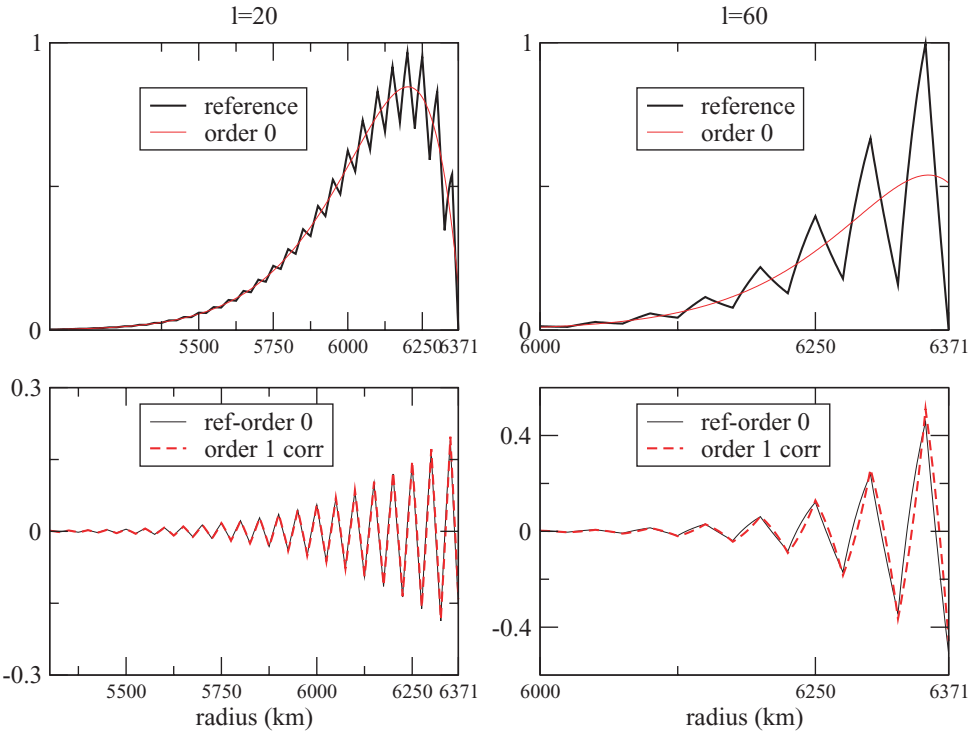

Figure 3. Minor m_5 (see eq. 11) of the two traction solutions in the spheroidal case computed for $l = 20$ (left column graphs) and $l = 60$ (right column graphs) in the original onion 1 model (see Fig. 2) (top graph, bold line, the 'reference' solution) and in the homogenized model (order 0, top graph thin line, the 'order 0' solution). On the bottom graphs is shown the order 1 periodic correction (dotted line) to be compared with the difference between the reference solution and the order zero solution (solid line).

In the following, we refer to (41) as the homogenized wave equation up to a given order (here 2). Furthermore, if we name $\hat{\boldsymbol{\mathcal{Y}}}^2(r) = (\mathbf{I} + \hat{\mathbf{X}}^2(\frac{r}{\varepsilon}))\langle\hat{\boldsymbol{\mathcal{Y}}}^2\rangle(r)$, where $\mathbf{I}$ is the identity matrix, one can check that $\boldsymbol{\mathcal{Y}}^\varepsilon = \hat{\boldsymbol{\mathcal{Y}}}^2 + O(\varepsilon^3)$.

Please note that $\mathbf{S}$ and therefore $\hat{\boldsymbol{\mathcal{Y}}}$ and $\mathbf{X}^i$ depend on the frequency ω (and on l). Solving (41) with (42–44) boundary conditions is done here by adapting the classical normal mode algorithm briefly described in Section 2. We solve (41) for different frequencies until (42–44) are satisfied with a shooting method. This adaptation should require a serious study of the operator $\langle\mathbf{S}\rangle + \varepsilon\langle\mathbf{S}\mathbf{X}^1\rangle + \varepsilon^2\langle\mathbf{S}\mathbf{X}^2\rangle$ and of the effect of the dynamic boundary conditions (42–44) on the eigenfrequency search scheme. This work will not be done here, and we just hope that the modifications do not perturb too much the classical eigenfrequency search algorithm. One can probably find models for which this option will fail. Nevertheless, the higher homogenization terms amplitude decay with ε compared to the leading term and therefore it is reasonable to assume that they do not perturb too much the original equations. As we will see, this quick and dirty solution is good enough to show that the homogenization provides accurate upscaling rules. In practice, computing a normal mode catalogue requires to solve (41) for many l and many frequencies. Because $\mathbf{S}$ depends on both l and ω, computing $\langle\mathbf{S}\rangle$, $\mathbf{X}^1$, $\langle\mathbf{S}\mathbf{X}^1\rangle$, etc, for each l and ω of each step of the shooting method used for each eigenfrequency is computationally intensive. To avoid this problem, we write these operators as power expansions in l and ω for which each coefficient can be computed once for all. For example,

$$\mathbf{X}^1_l(r,\omega) = {}_0\mathbf{X}^1(r) + {}_1\mathbf{X}^1(r)\gamma_l + {}_2\mathbf{X}^1(r)\gamma_l^2 + {}_\rho\mathbf{X}^1(r)\omega^2, \qquad (46)$$

with $\gamma_l = \sqrt{l(l+1)}$ and where the matrix coefficients ${}_0\mathbf{X}^1$, ${}_1\mathbf{X}^1$, ${}_2\mathbf{X}^1$ and ${}_\rho\mathbf{X}^1$ can be computed analytically once for all l and ω. Of course, the expression of different terms of higher and higher order

homogenization need more and more higher terms in l and ω and are more and more difficult to compute analytically.

To summarize, to obtain the homogenized solution up to an order i, one first needs to solve the homogenized wave eq. (41) with the boundary conditions (42–44) up to the order i to obtain the average homogenized solution $\langle \hat{\boldsymbol{\mathcal{Y}}}^i \rangle$at the order i. Then the homogenized solution is obtained by applying the periodic corrector to $\langle \hat{\boldsymbol{\mathcal{Y}}}^i \rangle$:

$$\hat{\boldsymbol{\mathcal{Y}}}^i(r) = \left(\mathbf{I} + \hat{\mathbf{X}}^i\left(\frac{r}{\varepsilon}\right)\right)\langle \hat{\boldsymbol{\mathcal{Y}}}^i \rangle(r) \tag{47}$$

In that case, we have $\boldsymbol{\mathcal{Y}}^\varepsilon = \hat{\boldsymbol{\mathcal{Y}}}^i + O(\varepsilon^i)$.

In the following examples as well as in the examples that will be done in the non-periodic case, we compare results obtained with the homogenized equation (41) with boundary conditions (42–44) at the same order (up to 2) with a reference solution. Because its expression similar to (46) is difficult to analytically compute and with minor effects in practice, the order 2 term $\langle \mathbf{S}\mathbf{X}^2 \rangle$ of the homogenized wave eq. (41) is neglected in the following. Therefore, when the order 2 is used, it only affects the boundary conditions through (42–44). Furthermore, because the first-order term of the homogenized equation $\langle \mathbf{S}\mathbf{X}^1 \rangle$ is zero for most of the regular earth models, using higher-order homogenization often consists in using the order 0 homogenized equation with higher order boundary conditions.

3.2 Examples

To illustrate this theoretical development, we give here two examples in 'earth' models with periodic variation of elastic properties as a function of r. To compute the reference solution, a classical normal mode algorithm is used to solve (7) in the original model. Knowing the accuracy of the normal mode solution, the reference solution is assumed to be 'exact'. We then solve (41) with (42–44) boundary conditions by adapting the same algorithm to this slightly different equation and different boundary conditions as mentioned in the previous section.

In this section, we first show a first example in a periodic model in which the first-order term of the homogenized wave equation $\langle \mathbf{S}\mathbf{X}^1 \rangle$is zero and a second (unusual) with $\langle \mathbf{S}\mathbf{X}^1 \rangle \neq 0$.

The first model used to test this homogenization, shown in Fig. 2, is made of homogeneous isotropic layers with $\lambda_m = 50$ km. The order 0 homogenized model is also shown in Fig. 2 (right plot). It is homogeneous but anisotropic, even if the original model is isotropic. It appears that for this model, we have $\langle \mathbf{S}\mathbf{X}^1 \rangle = 0$. Because it controls the eigenfrequency search, we first look at the m_5 minor (see Section 2, eq. 11) as a function of the radius in Fig. 3. The m_5 minor may not be easy to interpret physically, but similar figures would be obtained using one component of the traction (e.g. T_U of eq. 6). In the toroidal case, the m_5 minor is indeed the radial traction. Fig. 3 is constructed the following way: we first find the first eigenfrequency ${}_0\omega_l$ (fundamental mode) in the original model for a given l (here 20 and 60). We then compute m_5 and its correction for the homogenized equation and model up to the wanted order (here 1) for the fixed frequency ${}_0\,\omega_l$. Note that, fixing the eigenfrequency to the value computed in the original model is just done here for the purpose of the Figs 3, 4 and 8 only and is not used for other tests. The two top graphs show the reference m_5 computed with the original eq. (7) and the homogenized m_5 for the order 0. The order 0 is clearly an average of the reference solution. One can see that order 0 solution does not vanish at the free surface as it is the case for reference solution (this is more obvious for $l = 60$). This clearly indicates that this frequency is an eigenfrequency of the original problem,

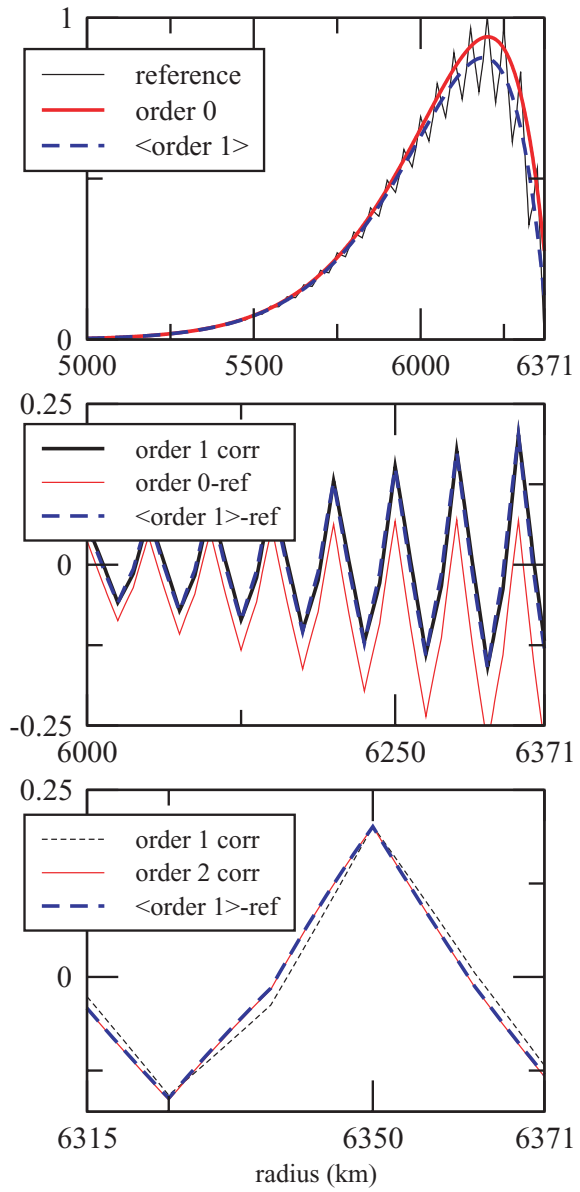

Figure 4. Minor m_5 (defined eq. 11) for $l = 20$ for a modified version of the onion 1 model (Fig. 2) for which $\langle \mathbf{S}\mathbf{X}^1 \rangle \neq 0$ (see text). On the top graph is shown the reference solution (thin line), the order 0 homogenized solution (bold line) and the order 1 average solution (broken line). In the middle graph is shown order 0 residual with respect to the reference solution (thin line), the order 1 residual (broken line) and the first-order periodic correction (bold line). On the bottom graph is shown a zoom of the middle graph where the order 2 periodic correction has been added (bold dotted line).

but not of the order 0 homogenized problem. As a consequence, searching eigenfrequencies for the order 0 homogenized problem gives a different set of eigenfrequencies compared to the original problem and does not allow to preserve important properties like the group velocity. The lower plots of Fig. 3 show a comparison between the residual of the reference solution and the order 0 solution and the first-order correction. It can be seen that the two curves match well for $l = 20$. The match is not as good for $l = 60$, but this is expected as ε increases with l (the wavelength is directly linked to l). Please note that here (the frequency is fixed) the order 0 average solution is the same as the order 1 because $\langle \mathbf{S}\mathbf{X}^1 \rangle = 0$. This is why the residual of the reference solution with the order 0 solution matches with the

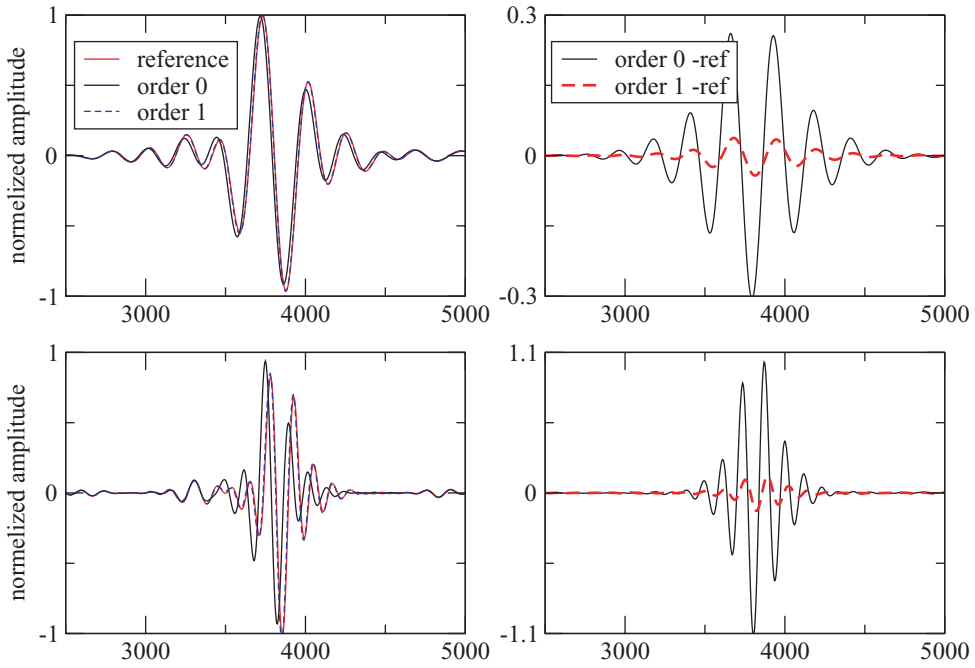

Figure 5. Vertical component synthetic seismograms computed in the onion 1 model (see Fig. 2). The source is a vertical force with a frequency cut-off at 1/200 Hz for the two top graphs and 1/100 Hz for the two bottom graphs. The epicentral distance is of 132° and the graphs are centred on the *R*1 Rayleigh wave time window. On the two left graphs are shown the reference solution, the order 0 homogenized solution and the order 1 average solution. On the two right graphs are shown the residual between the order 0 homogenized and the reference solutions and between the order 1 and the reference solution. The two lower plots have the same legend as the two upper ones.

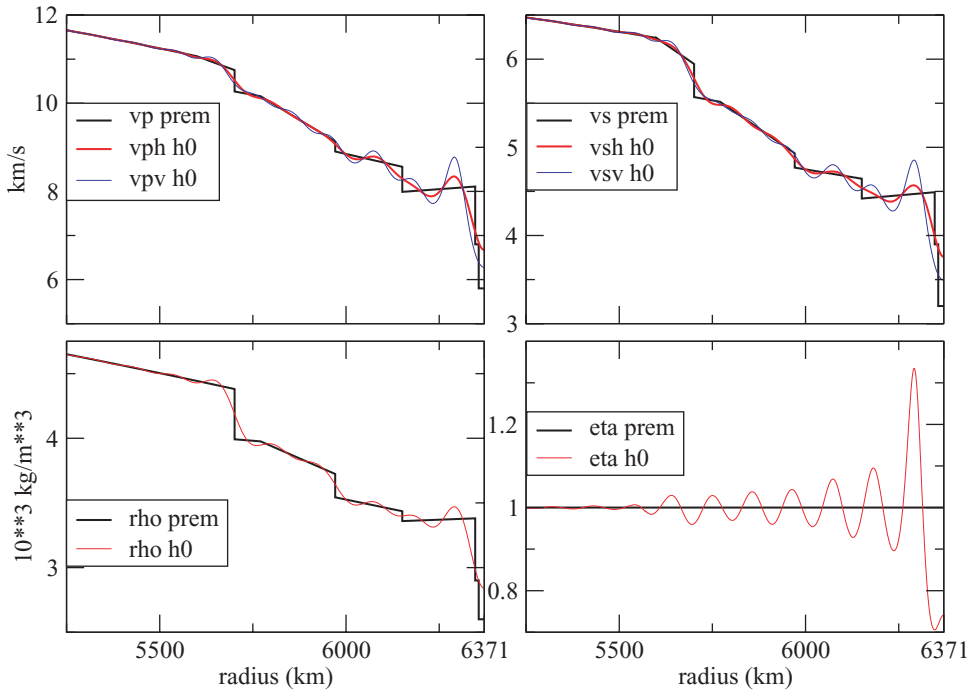

Figure 6. Isotropic Preliminary Earth Model (PREM) model and its homogenized version the order 0 (h0) build with the 'symmetric' extension. . V_{ph} and V_{pv} (upper left plot), V_{sh} and V_{sv} (upper right plot), density (lower left plot) and η (lower right plot) for both models are represented as a function of the radius. The lower pass filter $w(r)$ chosen here has a flat wave number spectrum between 0 and 1/120 km^{-1} and cosine taper between 1/120 km^{-1} and 1/100 km^{-1} and zero after 1/100 km^{-1}.

first-order periodic correction. In the case of $\langle \mathbf{SX}^1 \rangle \neq 0$, only the residual of the reference solution with the order 1 solution could match with the first-order periodic correction. For this example, the first-order correction accurately improve the order 0 solution and therefore the boundary condition at the order 1 allows to find an eigenfrequency with a better accuracy than using the order 0 only.

The second test is performed in a model for which $\langle \mathbf{SX}^1 \rangle$is not 0. To do so, we use a similar model as shown Fig. 2, but this time,

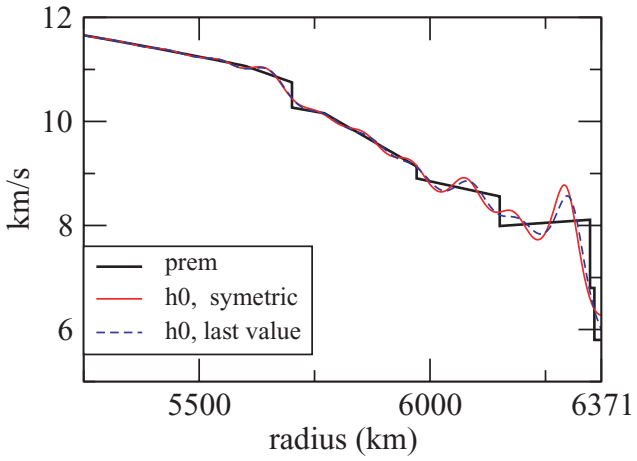

Figure 7. V_{ph} velocities for PREM, for h0 (the order 0 homogenized PREM build with the 'symmetric' extension) and for h0$_l$ (the order 0 homogenized PREM build with the 'last value' extension) The other quantities of the model (V_{pv}, V_{sh}...) show similar patterns.

V_{ph} and V_{pv} as well as V_{sh} and V_{sv} are still periodic and of the same shape as shown Fig. 2 but not in phase by 12.5 km. This gives an unusual isotropic model as the V_{xh} (where x stands for p or s) discontinuities do not match the V_{xv} discontinuities. This is the only type of model we have tried for which $\langle \mathbf{SX}^1 \rangle \neq 0$. In Fig. 4 is show again m_5 minor for $l = 20$, but in the modified model. It can be seen that the order 1 periodic correction (middle graph) only fit the residual of the order 1 average solution ($\langle \hat{\boldsymbol{\mathcal{Y}}}^1 \rangle$) with respect to the reference solution. This is not the case when the residual is computed with respect to the order 0 solution. This makes clear that taking into account $\langle \mathbf{SX}^1 \rangle$ when different from zero in (41) is required to obtain a correct result. Finally, on the bottom graph is shown a zoom of the middle graph where the order 2 periodic correction has been added. It can be seen that order 2 perfectly matches the residual between the order 1 average solution and the reference solution (which indicates that the order 2 term of the homogenized wave equation $\langle \mathbf{SX}^2 \rangle$ has a negligible effect on the average solution for this model and for this eigenfrequency).

Now that we are able to compute minors solution for the homogenized equation and we have checked that the periodic correction provides the correct boundary conditions, we are able to compute an homogenized normal mode basis. With this homogenized basis, we can compute synthetic seismograms according to (12). Doing so, we obtain a set of eigenfrequencies at the order i and the average of the eigenfunction $\langle \hat{\boldsymbol{\mathcal{Y}}} \rangle$ also at the order i. To be fully consistent, we should correct the normal mode solution with the periodic corrections according to (47) at the source and receiver location. We neglect this correction here. This is an order 0 approximation (we indeed have $\boldsymbol{\mathcal{Y}}^\varepsilon = \langle \hat{\boldsymbol{\mathcal{Y}}}^0 \rangle = \hat{\boldsymbol{\mathcal{Y}}}^0$ at the order 0). We shall see later that this approximation doesn't hold any longer for double couple sources, but performs well for force sources. In Fig. 5 are shown vertical component traces obtained at an epicentral distance of 132° from a vertical source force for two different frequency cut-offs: $f_{c1} = 1/200$ Hz (two top graphs) and $f_{c2} = 1/100$ Hz (two bottom graphs). In the volume, we have roughly $\varepsilon \simeq 1/14$ in the first case and $\varepsilon \simeq 1/7$ in the second case. The estimation of ε is probably too optimistic as the variation with depth of surface waves is sharper than the minimum wavelength. We expect a better result for f_{c1} than for f_{c2}. This is indeed the case in Fig. 5. We see that using order 0 only leads to an incorrect Rayleigh wave phase speed. The wave speed is corrected by using the order 1, which is here, because $\langle \mathbf{SX}^1 \rangle = 0$, only a boundary condition correction. To obtain a more precise result or to go to higher frequency, one should consider homogenization to order higher than one.

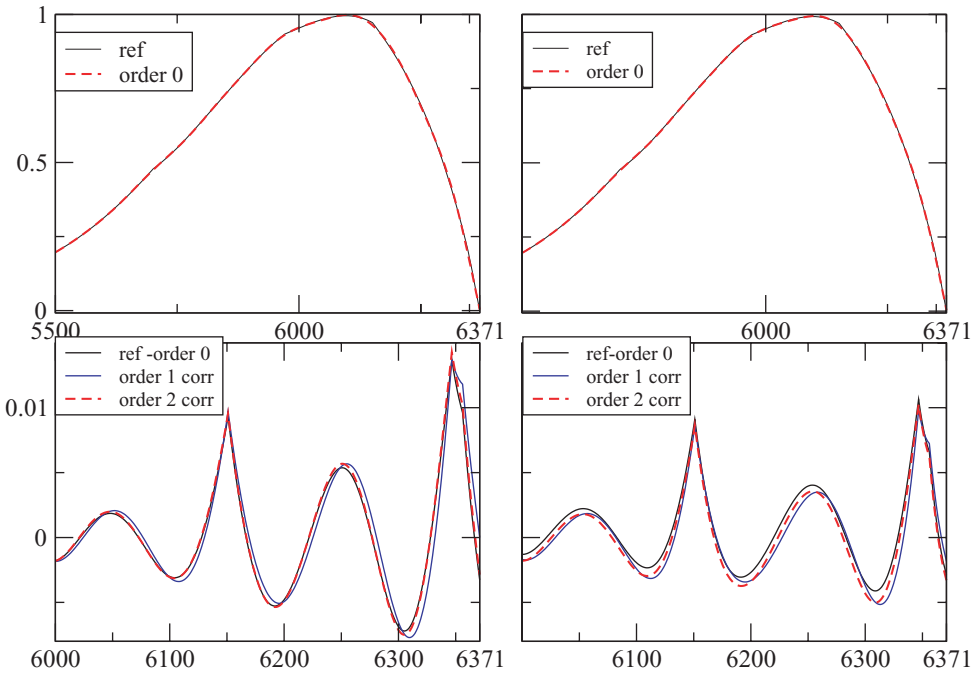

Figure 8. Minor m_5 (see eq. 11) of the two traction solutions computed in the h0 (left column plots) and in the h0$_l$ (right column plots) homogenized PREM for the first eigenfrequency of $l = 20$. On the two top plots is shown the solution computed in PREM ('ref') and the homogenized solution at the order 0. On the two lower plot is shown the residual between the reference and the order 0 solutions and compared with the order 1 and 2 periodic corrections. In that case, the periodic correctors are not periodic in r anymore.

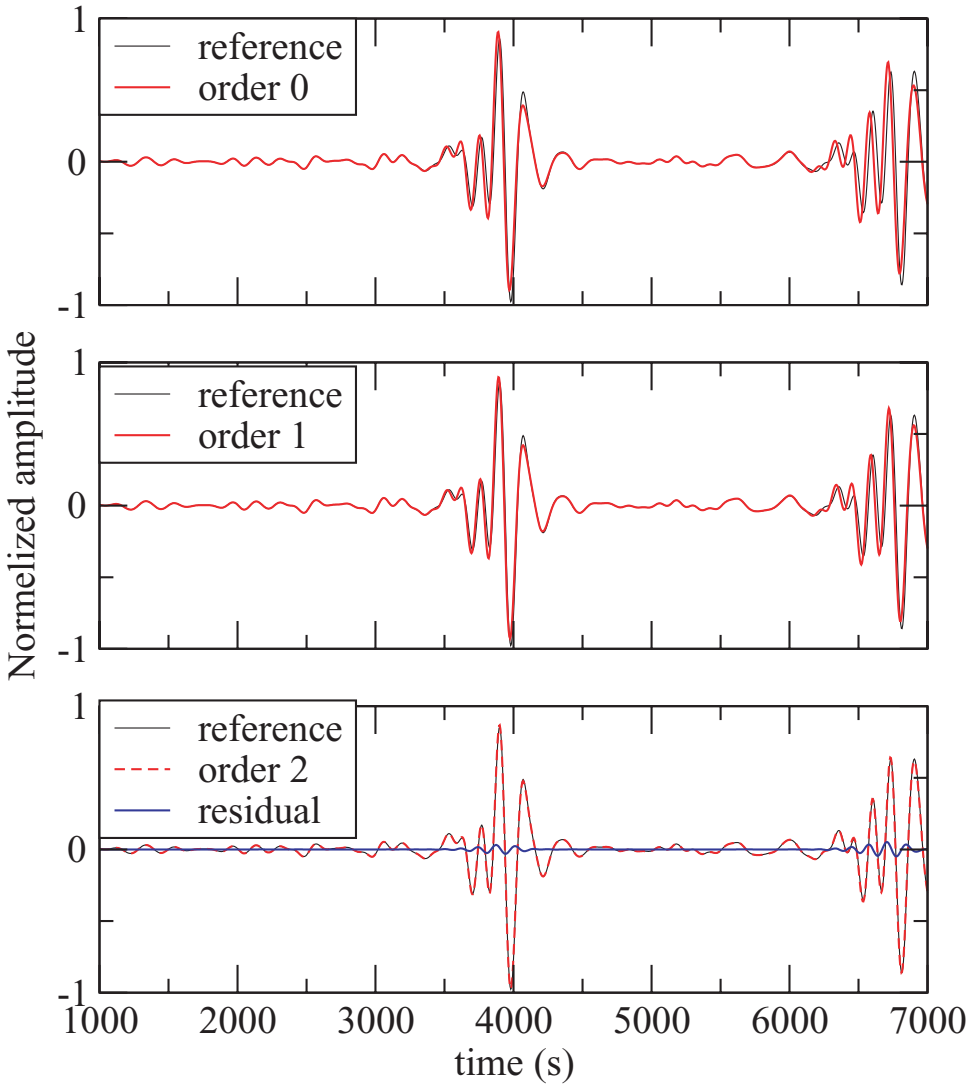

Figure 9. Vertical component of the displacement due to a vertical force at 221 km depth recorded at an epicentral distance of 132°. The 'reference' solution is computed in the PREM model and homogenized solutions at the order 0, 1 and 2 computed with last value extension are shown. A zoom of the R1 train of the same solutions is show Fig. 10.

4 APPLICATION TO THE NON-PERIODIC CASE

4.1 Theoretical development

We now relax the λ_m-periodicity condition on the elastic coefficients. Nevertheless, we keep the idea of separating microscopic scales from macroscopic scales by introducing a small parameter $\varepsilon = \frac{l_0}{\lambda_c}$, where l_0 is a length, that remains to be chosen, smaller than λ_c and a fast variable $y = \frac{r-r_\Omega}{\varepsilon}$. In the periodic case, the natural choice is $l_0 = \lambda_m$, but this option is not available here and an arbitrary choice has to be made. Any l_0 can be valid as long as ε is small compared to 1, knowing that this choice will affect the accuracy of the result. To be able to use the same set of equations as developed in the periodic case, we need to build an operator $\mathbf{S}(r, y)$ periodic in y. There is an infinite number of possibilities to build $\mathbf{S}(r, y)$ as an extension of $\mathbf{A}^\varepsilon$ such that $\mathbf{S}(r, \frac{r-r_\Omega}{\varepsilon}) = \mathbf{A}^\varepsilon(r)$ and periodic in y. We experiment with only one possibility in this paper that we refer to as the 'continuous' periodic extension (Laptev 2005). We show this choice gives accurate results, but this is not the only option and other choices may give different and interesting results.

To build this continuous extension, we need first $\mathbf{A}^\varepsilon$ to be extended for $r > r_\Omega$. Once again many choices are possible for this extension. We experiment with two options here:

(i) the symmetric extension: $\mathbf{A}^\varepsilon(r) = \mathbf{A}^\varepsilon(2r_\Omega - r)$ for $r > r_\Omega$;
(ii) the 'last value' extension: $\mathbf{A}^\varepsilon(r) = \mathbf{A}^\varepsilon(r_\Omega)$ for $r > r_\Omega$.

We introduce a 'smooth' version of $\mathbf{A}^\varepsilon(r)$, $\mathbf{A}^s(r)$, which will be defined later, and a 'fast' version, $\mathbf{A}^f(r) = \mathbf{A}^\varepsilon(r) - \mathbf{A}^s(r)$. Let $L(r)$ be a segment of length l_0 around r: $L(r) = [r - \frac{l_0}{2}, r + \frac{l_0}{2}]$.

(i) First, we define an auxiliary function $\tilde{\mathbf{S}}(r, .)$ for $r' \in L(r)$: $\tilde{\mathbf{S}}(r, r') = \mathbf{A}^f(r')$.
(ii) Second, we extend $\tilde{\mathbf{S}}(r, .)$to the whole real axis by periodicity. $\tilde{\mathbf{S}}(r, r')$ is now l_0-periodic for r'.
(iii) Finally, we define

$$\mathbf{S}(r, y) = \mathbf{A}^s(r) + \tilde{\mathbf{S}}\left(r, \frac{r - r_\Omega}{\varepsilon}\right). \tag{48}$$

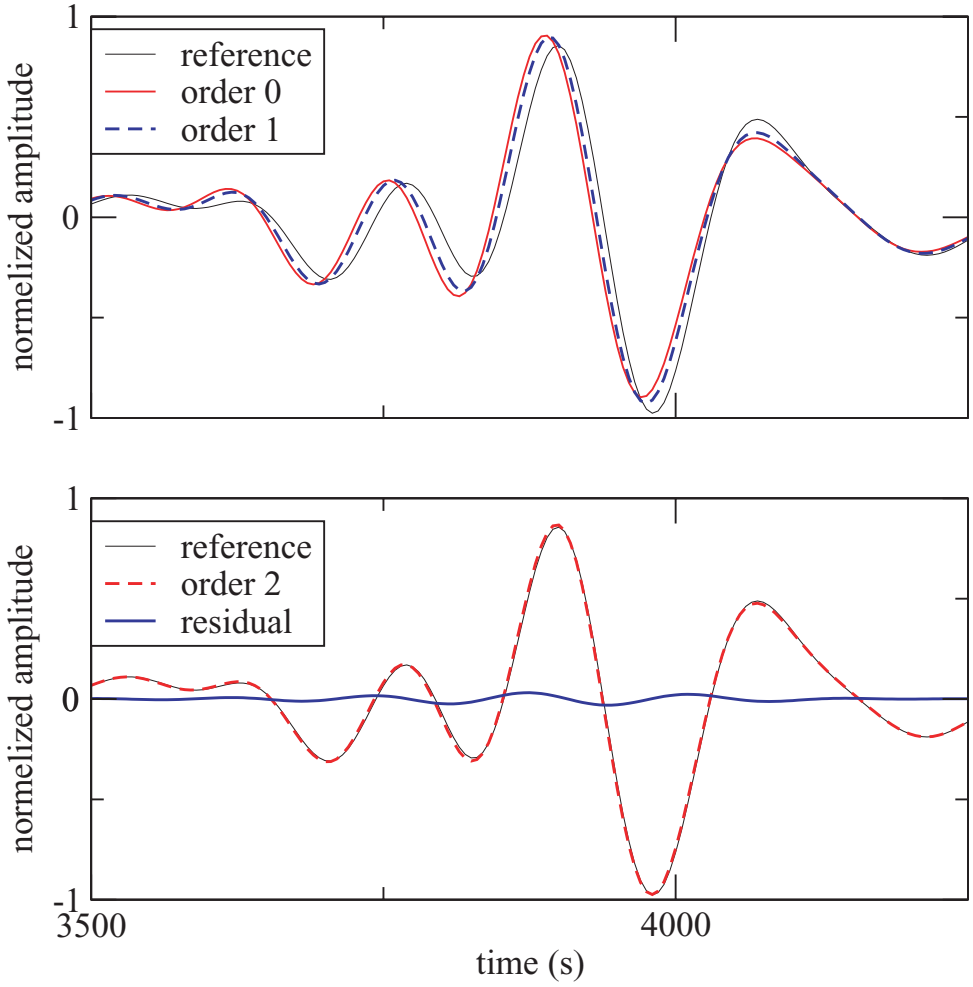

Figure 10. Same as Fig. 9 but zoomed on the R1 phase.

In other words, $\mathbf{S}(r, y)$is built from the original operator by, for each r, taking a window of length l_0 around r and extending it by periodicity. With such a definition, we indeed have $\mathbf{S}(r, \frac{r-r_\Omega}{\varepsilon}) = \mathbf{A}^\varepsilon(r)$, with $\mathbf{S}(r, y)$ λ_c-periodic in y with $\lambda_c = \frac{l_0}{\varepsilon}$.

Now that $\mathbf{S}$ $(r, y)$is defined, we can derive the same two-scale formalism as for the periodic case and obtain the same system of equations (41). The difference is that the correctors $\mathbf{X}^i$ which depend only on y in the periodic case now depend on both r and y. The boundary conditions for (41) are therefore slightly different than for the periodic case:

$$\left[\langle {}_s\hat{\boldsymbol{\mathcal{Y}}}^i\rangle(r_{\boldsymbol{\Omega}})\right]_2 = -\left[{}_s\hat{\mathbf{X}}^i(r_{\boldsymbol{\Omega}}, 0)\langle {}_s\hat{\boldsymbol{\mathcal{Y}}}^i\rangle(r_{\boldsymbol{\Omega}})\right]_2, \tag{49}$$

$$\left[\langle {}_s\hat{\boldsymbol{\mathcal{Y}}}^i\rangle(r_{\boldsymbol{\Omega}})\right]_4 = -\left[{}_s\hat{\mathbf{X}}^i(r_{\boldsymbol{\Omega}}, 0)\langle {}_s\hat{\boldsymbol{\mathcal{Y}}}^i\rangle(r_{\boldsymbol{\Omega}})\right]_4, \tag{50}$$

$$\left[\langle {}_t\hat{\boldsymbol{\mathcal{Y}}}^i\rangle(r_{\boldsymbol{\Omega}})\right]_2 = -\left[{}_t\hat{\mathbf{X}}^i(r_{\boldsymbol{\Omega}}, 0)\langle {}_t\hat{\boldsymbol{\mathcal{Y}}}^i\rangle(r_{\boldsymbol{\Omega}})\right]_2. \tag{51}$$

The choice of the 'smooth' operator $\mathbf{A}^s$now needs to discussed. One obvious choice is $\mathbf{A}^s = 0$. In that case, the homogenization would give an as accurate result as any other choice, but the order 0 homogenized model defined by $\langle \mathbf{S} \rangle$ may not be adapted for many numerical methods. Indeed, one of the advantages of the homogenization is to remove discontinuities so that they do not need to be meshed anymore. If the original elastic model has one zero-order discontinuity (a step), then the homogenized model would have two first-order discontinuities (discontinuities in the first derivatives: a slope). From the meshing point of view, the homogenized model is not easier to mesh than the original one. A solution to this problem would be to reiterate the homogenization (to homogenize the homogenized model). We will not explore this solution here. Instead, we choose a smooth $\mathbf{A}^s$such that $\langle \tilde{\mathbf{S}}(r, \varepsilon y)\rangle$ is small and can be neglected and therefore $\langle \mathbf{S} \rangle \simeq \mathbf{A}^s$. If $\mathbf{A}^s$ does not contain any discontinuity, the meshing problems are cleared. Such an $\mathbf{A}^s$ can be built as $\mathbf{A}^s = \mathbf{A}^\varepsilon * w$ where $*$ is the space convolution and $w(r)$ a low-pass filter wavelet with a corner wave-number sufficiently larger than $\frac{1}{l_0}$. In that case, we indeed have $\langle \mathbf{A}^\varepsilon - \mathbf{A}^s \rangle \simeq 0$.

4.2 Examples

In order to test this homogenization in the non-periodic case, we use the popular Preliminary Earth Model (PREM) (Dziewonski & Anderson 1981) model in its isotropic version and without ocean. This choice is arbitrary and any other non-periodic model with thin layer compared to the wavelength close to the surface would have been convenient for these tests. We build the smooth model using a low-pass filter w with a unit flat wave-number spectrum between 0 and 1/120 km^{-1} and cosine taper between 1/120 km^{-1} and

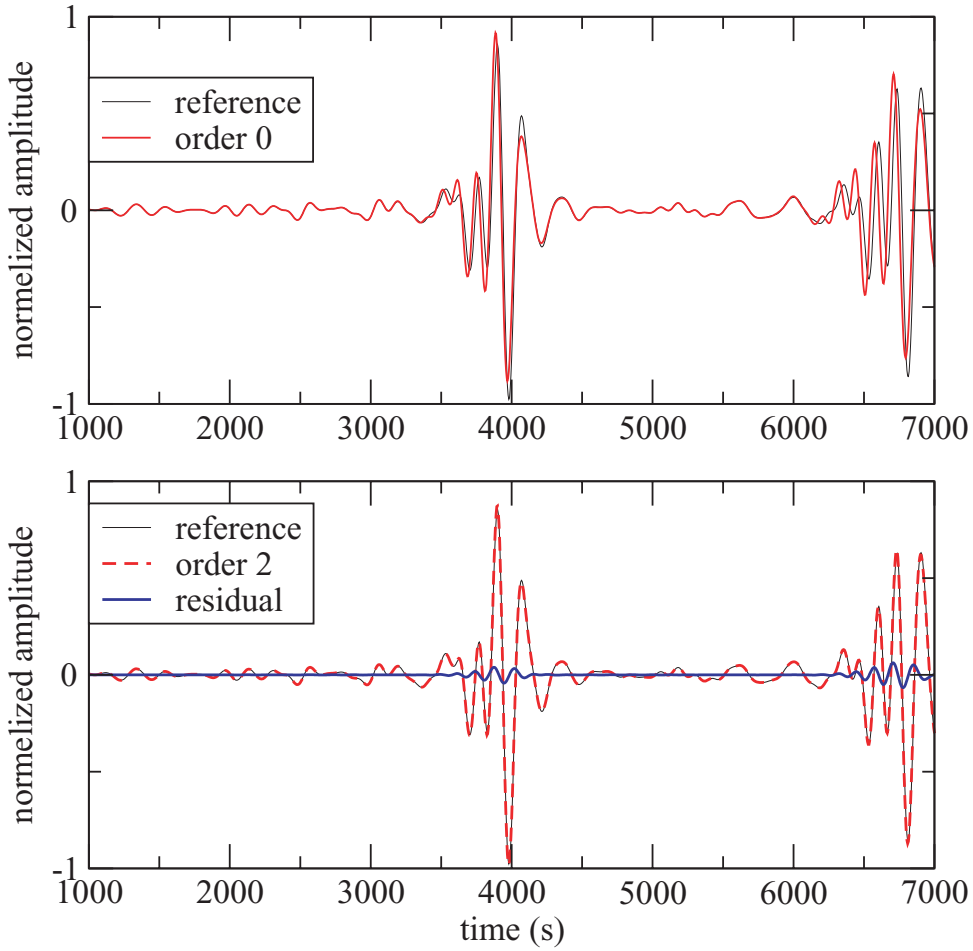

Figure 11. Same as Fig. 9 but this time, the homogenization has been performed with the symmetric extension. In that case, the order 0 is also the order 1 which explain why no 'order 1' solution is plotted. The time-shift, for the first Rayleigh phase, between the the order 0 homogenization and the reference solution (top plot) is about 13 s.

1/100 km^{-1} and zero after 1/100 km^{-1}. Such a homogenization removes all scales smaller than 100 km from the model. We name the resulting order 0 homogenized model built with the symmetric extension 'h0' and 'h0$_l$' the one obtained with the last value extension. The h0 model is shown in Fig. 6. A comparison between h0 and h0$_l$is shown in Fig. 7 for V_{ph}. Once again the homogenized model is anisotropic even though the original model is isotropic. The homogenized model is oscillatory, which was not the case of PREM, but, as expected, is smooth. The models obtained from different extensions above the Earth surface are different which shows that the homogenized model is not unique and depends upon choices made for the homogenization. Here again, it appears that the first- order term of the homogenized wave equation $\langle \mathbf{SX}^1 \rangle$ is zero.

In Fig. 8 is shown one example of m_5 minor computed in PREM and in the h0 homogenized model (right plots), in the h0$_l$homogenized model (left plots) for $l = 20$. In that case, the 'periodic' correctors are not periodic anymore. For the symmetric extension, the order 2 boundary correction gives a good correction of the order 0 homogenized equation. This means that the order 2 term of the homogenized equation has a weak effect and that $\langle \hat{\mathcal{Y}}^2 \rangle$ is negligible. For the last value extension (right plots) things are different, as the order 2 correction has a closer shape to the order 0 correction than the order 1 correction,but with a smooth offset. This is a clear indication that the order 2 term ($\langle \mathbf{SX}^2 \rangle$) of the homogenized equation (41) is not negligible and that it should be used here. It can be seen that the order 1 periodic correction falls to 0 at the free surface for the symmetric extension case. It appears to be general, when the symmetric extension is used, the periodic correctors are zero at the surface. No modification of the boundary condition is required at the order 1 in that case. As in most of the cases, the first-order homogenized equation term ($\langle \mathbf{SX}^1 \rangle$) is zero and, if the symmetric extension is used, the order 0 solution is therefore already at the order 1.

Thanks to these correctors, we are now able to build a normal mode basis for the homogenized model and equations. Figs 9 and 10 show the vertical component waveforms in the last value extension case. The source is a vertical force at 221 km depth at an epicentral distance of 132°. The corner frequency of the source is 1/100 Hz. It appears that even if the order 1 provides a better result than the order 0, the order 2 is required to obtain a correct phase velocity of the surface waves. Fig. 11 shows the same numerical experiment in the case of the symmetric extension. The order 1 solution has not been represented, since it is the same as the order 0. Once again, the order 2 provides an accurate result.

So far, we have only used a vertical force source. Earthquake sources are better represented by double couple sources. As shown by eq. (13), such a source requires to compute the strain tensor $\boldsymbol{\epsilon}$ and therefore the first derivative with respect to r of the solutions.

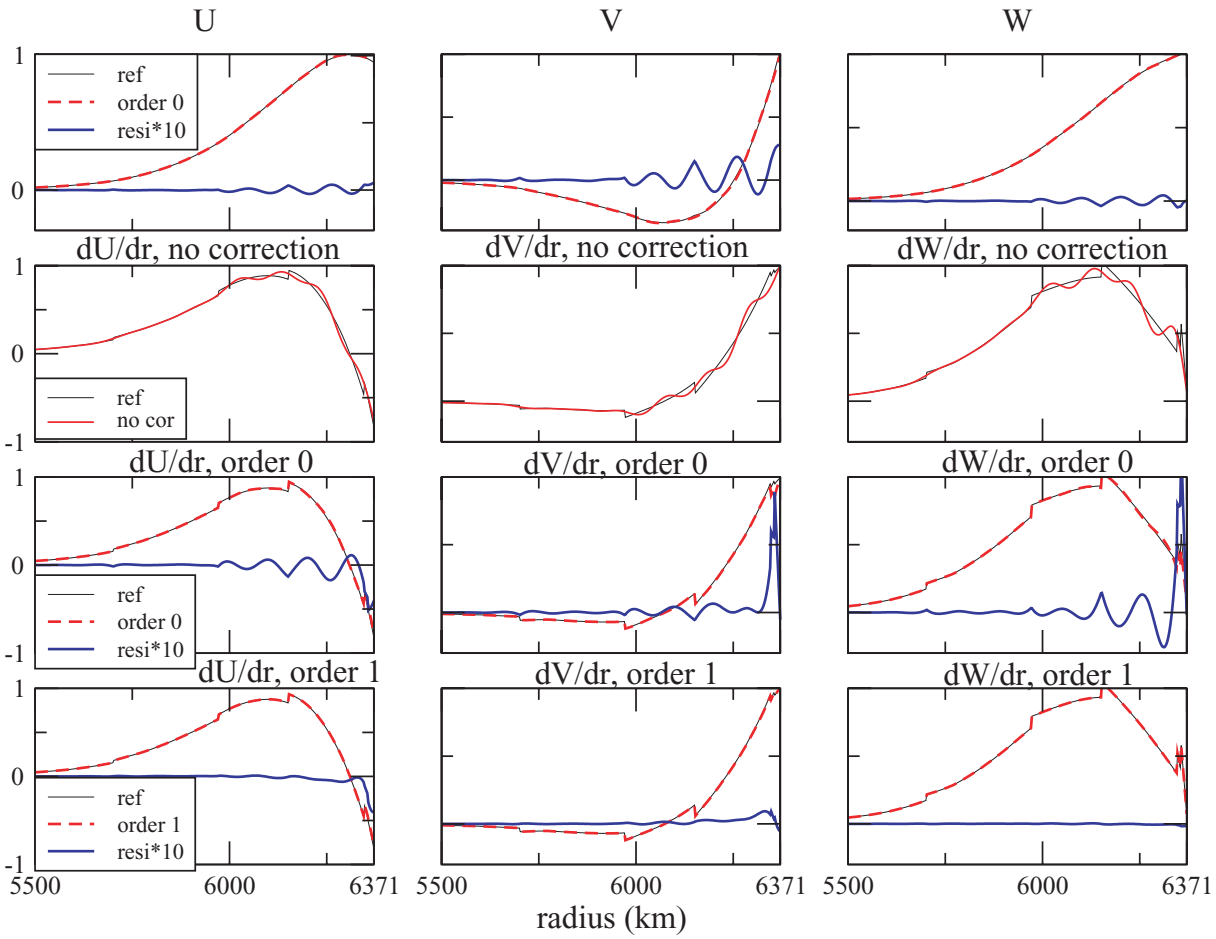

Figure 12. Fundamental mode solution U, V and W components and their derivative with respect to r for $l = 50$ computed in PREM and in h0 homogenized model computed with the symmetric extension (Fig. 6). The 'ref' legend stands for the reference solution computed in the original model. The 'resi*10' stands for the residual between the homogenized solution at a given order times 10. The first line of plots shows the three components of the average homogenized displacement computed at the order 2. The three following lines of plots show the displacement first-order derivative with respect to r of the reference solution and of the average homogenized solution at the order 2, and then when applying the order 0 and to the order 1 order periodic correction.

Even at the order 0 for which the solution does not depend on y, its derivative with respect to r depends on y:

$$\frac{\partial \boldsymbol{\mathcal{Y}}^{\varepsilon}}{\partial r} = \frac{\partial \boldsymbol{\mathcal{Y}}^{0}}{\partial r} + \frac{\partial \boldsymbol{\mathcal{Y}}^{1}}{\partial y} + O(\varepsilon), \tag{52}$$

$$= \langle \mathbf{S} \rangle \boldsymbol{\mathcal{Y}}^{0} + \frac{\partial \boldsymbol{\mathcal{X}}^{1}}{\partial y} \boldsymbol{\mathcal{Y}}^{0} + O(\varepsilon), \tag{53}$$

$$= \mathbf{S} \boldsymbol{\mathcal{Y}}^{0} + O(\varepsilon). \tag{54}$$

where $\mathbf{S}$ is taken in $(r, \frac{r}{\varepsilon})$. At the order 0, we have $\boldsymbol{\mathcal{Y}}^{0} = \langle \boldsymbol{\mathcal{Y}} \rangle$ and therefore

$$\frac{\partial \boldsymbol{\mathcal{Y}}^{\varepsilon}}{\partial r} = \mathbf{S} \langle \boldsymbol{\mathcal{Y}} \rangle + O(\varepsilon). \tag{55}$$

Because $\mathbf{S}$ depends on y, $\frac{\partial \boldsymbol{\mathcal{Y}}^{\varepsilon}}{\partial r}$ also depends on y at the order 0 and therefore varies rapidly. At the order one, we find

$$\frac{\partial \boldsymbol{\mathcal{Y}}^{\varepsilon}}{\partial r} = \mathbf{S}(\mathbf{I} + \varepsilon \mathbf{X}^{1}) \langle \boldsymbol{\mathcal{Y}} \rangle + O(\varepsilon^{2}). \tag{56}$$

To illustrate this point, Fig. 12 shows solutions U, V and W as defined by (5) and their derivatives with respect to r computed in PREM and in the homogenized PREM with the symmetric extension. For the homogenized solution, the eigenfrequency is computed up to the order 2. On the top plots is shown the displacement without applying any periodic correction. The residual times 10 shows that the homogenized solution is accurate, even without the periodic correction. This explains why, once the normal mode basis is computed at the order 2, we can forget the corrections at the receiver and the source location in the case of a force source. In the case of a double couple, things are different. Indeed, as already mentioned, the moment tensor interacts with the strain and not the displacement. In that case, derivatives with respect to the radius of the solutions are required and it can be seen that, if no correction is applied to the homogenized solution, the solutions are not accurate for the derivatives (Fig. 12, second line of plots). It also appears that for sources close to the surface, the order 0 correction might not be enough (Fig. 12, third line of plots). Finally, the order 1 gives an accurate result (Fig. 12, last line of plots).

Figs 13 and 14 shows the vertical and transverse components of the displacement due to a double couple point source at 11 km depth recorded at an epicentral distance of 132°. Here, the eigenfunction set is found by using the order 2 homogenization for the boundary conditions. With this basis, the source term is used without correction (top plots), with the order 0 correction (middle plots) and the order 1 (bottom plots). For this shallow source and this moment

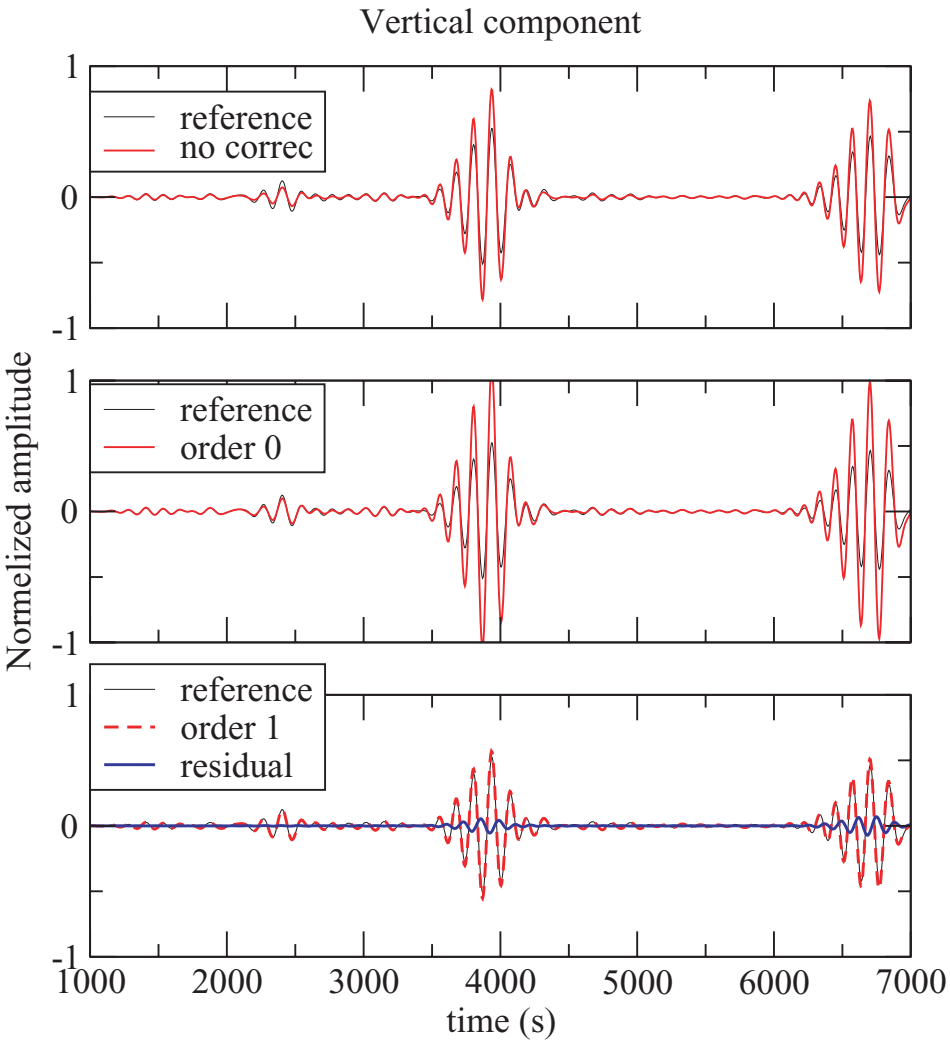

Figure 13. Vertical component of the displacement due to a double couple point source at 11 km depth recorded at an epicentral distance of 132°. The 'reference' solution is computed in the PREM model and homogenized solutions are all computed using order 2 homogenized average eigenfunction. The homogenized solution are computed without (top graph), with order 0 (middle graph) and with order 1 correction for the source (bottom graph).

tenor, the order 1 correction is required to obtain an accurate result. In many cases (e.g. deeper source) the 0 order correction is enough. An interesting point of the order 0 correction at the source is that it still gives a local source (that can be represented by an effective moment tensor, see Appendix B). At the order 1, the correction of the source is not local anymore by requiring higher order derivatives of the solution.

Finally, knowing that the Rayleigh wavelength is roughly about 400 km at 100 s period in PREM, the $\varepsilon \simeq 0.25$ which is not really small. One can see that the results are nevertheless good enough to work with data.

5 CONCLUSION AND PERSPECTIVES

We have applied a classical two-scale homogenization technique to the wave equation in layered media. We have shown that the order 0 homogenization provides the same result as the one previously obtained by Backus (1962). It appears that the order 0 is not enough to obtain an accurate solution especially for surface waves. Higher order homogenization terms (up to 2) allow us to obtain accurate surface waves. It appears that higher order homogenization often consists in a modification of the boundary condition which corrects for the inaccuracy observed for surface waves at the order 0. To solve the homogenized equation, we have adapted normal mode computation and normal mode summation programs. Of course, the main goal of the work initiated with this paper is not to use homogenization for 1-D media with normal mode algorithms, but for 3-D media with numerical schemes, such as the SEM method . In a first step, the equations found here could be converted from the frequency-spectral domain to the time-space domain (for example, $-\omega^2$is $\frac{d^2}{dt^2}$ and γ_l^2 is related to the horizontal laplacian ∇_1^2) in order to be used in SEM. Doing so, it could be, for example, directly applied to existing crustal models for which the horizontal properties are slowly varying (typically, boxes of 200 km length) compared to the vertical variation (down to some hundreds of metres).

The next step is to extend this work to 3-D rapidly varying medium. This will not be straightforward for (at least) two reasons. First, when the dimension of the medium is higher than one, the classical two scale homogenization leads to a rapidly varying boundary condition. This boundary layer effect needs another asymptotic expansion close to the boundary of the medium to be matched with the one in the volume of the medium. Second, in the case of

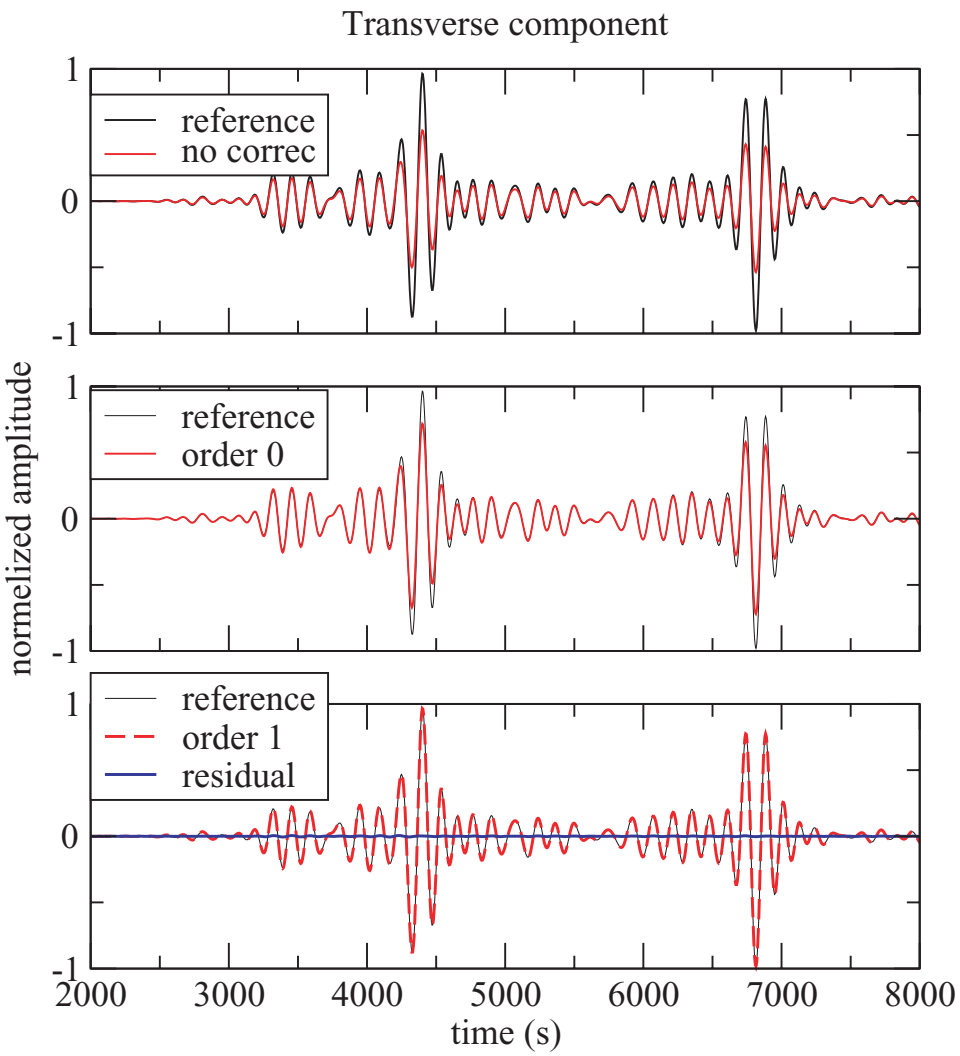

Figure 14. Same as Fig. 13, but for the transverse component.

non-periodic media, the introduction of the smooth operator used here may be complicated by the fact that the relation between the original and the order 0 homogenized media is not explicit anymore, but implicit. Nevertheless, once achieved, this work will considerably simplify the meshing issue for some numerical methods and in many cases.

For the inverse problem, this work and its future extension to 3-D models will allow us to build a smooth parametrization consistent with the smallest wavelength used. It can already be seen with this 1-D case that one should look for a transverse isotropic model, even if the real model is known to be made of isotropic layers. It also allows us to build a smooth starting model consistent with an existing layered model like PREM. This is important because it solves the problem of *a priori* miss-located interfaces. Finally, it appears that the coefficients of the boundary condition should also be inverted. Doing so, a stable inverse problem without *a priori* information for the crust can be designed. Such an inversion would allow to obtain an homogenized model from seismic data. After this step, a strong difficulty remains: how to interpret such a model. Finding physically meaningful (with small scales) model compatible with the homogenized model is an other inverse problem highly non-linear and probably highly non-unique. This problem will be addressed in a future work.

ACKNOWLEDGMENTS

Many thanks to J.P. Vilotte for many discussions and leading the first author toward two-scale homogenization. Many thanks to A. Mangeney and O. Castelnau for making the link between the two authors. We thank J. Woodhouse for his help with adapting the mode count system in the normal mode program. The authors thank V. Farra and J.P. Montagner for helping with the manuscript and B. Romanowicz and an anonymous reviewer for their very useful comments. This work has been funded by the French ANR MUSE project under the BLANC program. Computations were performed on IPGP's cluster, IDRIS and CINES computers.

REFERENCES

Abdelmoula, R. & Marigo, J.-J., 2000. The effective behaviour of a fibre bridged crack, *J. Mech. Phys. Solids*, **48**(11), 2419–2444.

Aki, K. & Richards, P., 1980. *Quantitative Seismology: Theory and Methods*, Freeman, San Francisco.

Allaire, G., 1992. Homogenization and two-scale convergence. *SIAM J. Math. Anal.*, **23**, 1482–1518.

Allaire, G. & Conca, C., 1998. Boundary layers in the homogenization of a spectral problem in fluid–solid structures, *SIAM J. Math. Anal.*, **29**(2), 343–379.

Auriault, J. & Bonnet, G., 1985. Dynamique des composites élastiques périodiques, *Arch. Mech*, **37**(4–5), 269–284.
Auriault, J.-L. & Sanchez-Palencia, E., 1977. Étude du comportement macroscopique d'un milieu poreux saturé déformable, *J. Mécanique*, **16**(4), 575–603.
Backus, G., 1962. Long-wave elastic anisotropy produced by horizontal layering, *J. geophys. Res.*, **67**(11), 4427–4440.
Bensoussan, A., Lions, J.-L. & Papanicolaou, G., 1978. *Asymptotic Analysis of Periodic Structures*, North Holland.
Briane, M., 1994. Homogenization of a non-periodic material, *J. Math. Pures Appl. (9)*, **73**(1), 47–66.
Dahlen, F.A. & Tromp, J., 1998. *Theoretical Global Seismology*, Princeton University Press. NJ.
Dumontet, H., 1986. Study of a boundary layer problem in elastic composite materials, *RAIRO Modél. Math. Anal. Numér.*, **20**(2), 265–286.
Dziewonski, A.M. & Anderson, D.L., 1981. Preliminary reference earth model, *Phys. Earth planet. Inter.*, **25**, 297–356.
Fish, J. & Chen, W., 2004. Space-time multiscale model for wave propagation in heterogeneous media, *Comp. Meth. Appl. Mech. Engng*, **193**, 4837–4856.
Francfort, G.A. & Murat, F., 1986. Homogenization and optimal bounds in linear elasticity, *Arch. Rational Mech. Anal.*, **94**(4), 307–334.
Golowich, S.E. & Weinstein, M.I., 2003. Homogenization expansion for resonances of microstructured photonic waveguides, *J. Opt. Soc. Am. B.*, **20**(4), 633–647.
Haboussi, M., Dumontet, H. & Billoët, J., 2001a. On the modelling of interfacial transition behavior in composite materials, *Computational Materials Science*, **20**, 251–266.
Haboussi, M., Dumontet, H. & Billoët, J., 2001b. Proposed of refined interface models and their application for free-edge effect Interface Modelling in Laminated Composites for Free Edge Effect Analysis, *Composites Interfaces*, **8**(1), 93–107.
Hashin, Z. & Shtrikman, S., 1963. A variational approach to the elastic behavior of multiphase materials, *J. Mech. Phys. Solids*, **11**, 127–140.
Hill, R., 1965. A self–consistent mechanics of composit materials, *J. Mech. Phys. Solids*, **13**, 213–222.
Komatitsch, D. & Vilotte, J.P., 1998. The spectral element method: an effective tool to simulate the seismic response of 2d and 3d geological structures, *Bull. seism. Soc. Am.*, **88**, 368–392.
Laptev, V., 2005. Two-scale extensions for non-periodic coefficients.arXiv:math.AP/0512123.
Moskow, S. & Vogelius, M., 1997. First-order corrections to the homogenised eigenvalues of a periodic composite medium. a convergence proof, *Proc. Roy. Soc. Edinburgh Sect. A*, **127**(6), 1263–1299.
Murat, F. & Tartar, L., 1985. Calcul des variations et homogénéisation, in *Homogenization methods: theory and applications in physics (Bréau-sans-Nappe, 1983)*, Volume 57 of *Collect. Dir. Études Rech. Élec. France*, pp. 319–369. Paris: Eyrolles.
Sanchez-Palencia, E., 1980. *Non-homogeneous media and vibration theory*, Number 127 in Lecture Notes in Physics. Berlin: Springer.
Takeuchi, H. & Saito, M., 1972. Seismic surface waves, *Methods in computational Physics.*, **11**, 217–295.
Woodhouse, J.H., 1988. The calculation of eigenfrequencies and eigenfunctions of the free oscillations of the Earth and the Sun. in *Seismological algorithms*, pp. 321–370. ed. Doornbos, D.J., Academic Press, New York.

APPENDIX A: EXPRESSIONS FOR MATRICES $\mathbf{A}^\varepsilon$ OR $\mathbf{S}$

We use here the A, C, F, L, Nelastic parameters defined form wave speeds,

$V_{pv} = \sqrt{C/\rho}$ for vertical P waves,

$V_{sv} = \sqrt{L/\rho}$ for vertical S waves,

$V_{ph} = \sqrt{A/\rho}$ for horizontal P waves,

$V_{sh} = \sqrt{N/\rho}$ for horizontal S waves,

and $\eta = \frac{F}{A-2L}$. In the isotropic case, we have $A = C = \lambda + 2\mu$, $L = N = \mu$ and $\eta = 1$, where λ and μ are the Lamé elastic coefficients.

For the spheroidal case, we have

$$s\boldsymbol{A}_l^\varepsilon(r,\omega) = \begin{pmatrix} d/r & 1/C & e_l/r & 0 \\ -\rho\omega^2 + a & -d/r & -a\gamma_l/2 & \gamma_l/r \\ -\gamma_l/r & 0 & 2/r & 1/L \\ a\gamma_l/2 & -e_l/r & -\rho\omega^2 + b_l & -2/r \end{pmatrix} \tag{A1}$$

with

$$a = \frac{4}{r^2}\left(A - \frac{F^2}{C} - N\right), b_l = \frac{\gamma_l^2}{r^2}\left(A - \frac{F^2}{C}\right) - \frac{2N}{r^2},$$
$$d = 1 - \frac{2F}{C}, \qquad e_l = \gamma_l \frac{F}{C}.$$

In the toroidal case, we have:

$${}_t\boldsymbol{A}_l^\varepsilon(r,\omega) = \begin{pmatrix} 2/r & 1/L \\ -\rho\omega^2 + \Omega_l N/r^2 & -2/r \end{pmatrix}, \tag{A2}$$

with $\Omega_l = (l-1)(l+2)$.

From these expressions, one can see that the averaged quantities required to compute $\langle \mathbf{S} \rangle$are $\langle \frac{1}{C} \rangle$, $\langle \frac{1}{L} \rangle$, $\langle A - \frac{F^2}{C} \rangle$, $\langle \frac{F}{C} \rangle$ and $\langle N \rangle$which is different from the average of the A, C, F, L, Nelastic parameters. This is the same result as that obtained by Backus (1962). With such averaging rules, an isotropic layered model has an anisotropic average. For example, an isotropic layered model has $N = L$, but the average model in general won't because $\langle N \rangle$ and $\langle \frac{1}{L} \rangle$are different.

APPENDIX B: ORDER 0 CORRECTION OF THE MOMENT TENSOR

The relation between the original moment tensor $\mathbf{M}$ and the equivalent one for the order 0 homogenized model $\mathbf{M}^{h0}$ is

$$M_{rr}^{h0} = M_{rr}\frac{C^{h0}}{C} \tag{B1}$$

$$M_{\theta\theta}^{h0} = M_{\theta\theta} + M_{rr}\frac{F^{h0} - F}{C} \tag{B2}$$

$$M_{\phi\phi}^{h0} = M_{\phi\phi} + M_{rr}\frac{F^{h0} - F}{C} \tag{B3}$$

$$M_{r\theta}^{h0} = M_{r\theta}\frac{L^{h0}}{L} \tag{B4}$$

$$M_{r\phi}^{h0} = M_{r\phi}\frac{L^{h0}}{L} \tag{B5}$$

$$M_{\theta\phi}^{h0} = M_{\theta\phi} \tag{B6}$$

where C, F and L are the elastic parameters (defined in appendix A) evaluated at the source depth and C^{h0}, F^{h0} and L^{h0} the same elastic parameters for the order 0 homogenized model evaluated at the source depth. An interesting consequence of the above relations is that null trace moment tensors may have an explosive component (trace different form 0) in the homogenized model.